Sirt1 mediated regulation of p107 mitochondrial function controls muscle stem cell proliferative fates

Debasmita Bhattacharya[1,2], Oreoluwa Oresajo[1,2] and Anthony Scimè[1,2*]

1. Stem Cell Research Group

2. Molecular, Cellular and Integrative Physiology

Faculty of Health, York University,

Toronto, Ontario

M3J 1P3, Canada

* Corresponding author E mail: ascime@yorku.ca

Tel: 1 416 736 2100 ext 33559

Abstract

Muscle wasting diseases and aging are associated with impaired myogenic stem cell self-renewal and a diminished number of their proliferating and differentiating committed muscle progenitor cells (MPs). Importantly, distinct metabolic states govern how MPs proliferate and differentiate. Central to this is the regulation of energy generation between glycolysis in the cytoplasm and oxidative phosphorylation (Oxphos) in the mitochondria. However, the mechanisms that connect these energy provisioning centers to control cell behaviour remain obscure. Herein, our results reveal a mechanism by which mitochondrial-localized transcriptional co-repressor p107 governs MP proliferative capacity, under the control of NAD^+ dependent Sirt1 deacetylase. We found p107 directly interacts at the mitochondrial DNA promoter leading to repression of mitochondrial-encoded genes. This reduces the mitochondrial ATP generation capacity, by limiting the electron transport chain complex formation. Importantly, the amount of ATP generated by the mitochondrial function of p107 is directly associated to the cell cycle rate in vivo and in vitro. In vivo, p107 genetically deleted MPs had a faster proliferative capacity, whereas forced expression of p107 in the mitochondria blocked cell cycle progression. Sirt1, whose activity is dependent on the cytoplasmic by-product of glycolysis, NAD^+, directly interacts with p107 impeding its mitochondrial localization and function. Deletion of Sirt1 increased p107 mitochondrial localization, decreased MP mitochondrial Oxphos generation, concomitant with dampened cell cycle progression. Increasing the activity of Sirt1 had the opposite effect on p107 function. This metabolic control of cell cycle progression, driven by differential p107 mitochondrial function based on Sirt1 activity, establishes a new paradigm to manipulate muscle cell proliferative fates that is likely to extend to most other dividing cell types.

Introduction

In recent years, there has been an emerging realization that metabolism plays an active role in guiding and dictating how the cell will behave(Ghosh-Choudhary et al., 2020; Khacho et al., 2016; Ochocki and Simon, 2013; Porras et al., 2017). Central to this assertion is the interplay between metabolic states based on glucose metabolism by glycolysis in the cytoplasm with oxidative phosphorylation (Oxphos) in the mitochondria. Indeed, the cell cycle rate is dependent on the amount of total ATP generated from glycolysis and Oxphos(Martinez-Reyes et al., 2016; Mitra et al., 2009). In glycolysis, ATP is produced at a fast rate and the glycolytic pathway components might be used for the biosynthesis of nucleic acids, proteins, carbohydrates and lipids essential for cell proliferation(Folmes et al., 2012). On the other hand, Oxphos, which produces at least 10 times more ATP, is crucial for progression through the G1/S transition of the cell cycle(Gemin et al., 2005; Salazar-Roa and Malumbres, 2017). Hyperactivation of Oxphos in proliferating cells is critical for their advancement, whereas its down regulation delays or blocks progression to S phase(Martinez-Reyes et al., 2016; Mitra et al., 2009; Sweet and Singh, 1995; van den Bogert et al., 1986; Wheaton et al., 2014).

Importantly, it is uncertain how glycolysis and Oxphos work together during proliferation to regulate the yield of ATP necessary for cell division. Indeed, proliferating cells customize methods to actively reduce Oxphos under conditions of higher glycolysis(Locasale and Cantley, 2011). Fundamental to understanding this relationship is the cytoplasmic NAD^+/NADH ratio, which is a reflection of the energy generated by glycolysis. NADH is a by-product of glycolysis that might be used as a reducing reagent required for Oxphos. Whereas, NAD^+, a coenzyme in various metabolic pathways, is the oxidized form of NADH that can be made in glycolysis from the transformation of pyruvate to lactate. High levels of cytoplasmic NAD^+ activate the lysine sirtuin (Sirt) deacetylase family, including Sirt1, which thus acts as an energy sensor(Canto et al., 2015). Increased Sirt1 activity enhances

mitochondrial metabolism by deacetylating histones, transcription factors and cofactors that boost mitochondrial function. In contrast, decreased NAD^+/NADH and Sirt1 activity is associated with reduced mitochondrial function as observed in aging and metabolic diseases(Cerutti et al., 2014; Zhang et al., 2016).

In the mitochondria the capacity for ATP production is dependent on the five electron transport chain (ETC) complexes, which are made up of protein subunits derived from the nuclear and mitochondrial genomes(Martinez-Reyes and Chandel, 2020). The closed double-stranded circular mitochondrial DNA (mtDNA) encode genes located on both strands, which are referred to as the heavy (H) and light (L) strands. Their promoters are located in the large noncoding region termed the displacement loop (D-loop)(Gustafsson et al., 2016). The mitochondrial genome is essential to control energy generation by the ETC, as thirteen mitochondrial-encoded genes are functional components of four out of five ETC complexes. Crucially, mitochondrial genes are limiting for ATP production and inhibiting their translation can block the cell cycle in G1(Gemin et al., 2005; Lapuente-Brun et al., 2013; Martinez-Reyes et al., 2016; Mendelsohn et al., 2018; Mitra et al., 2009; Rodriguez-Enriquez et al., 2006; van den Bogert et al., 1986).

Mounting evidence has shown that Rb1/Rb and p107/Rbl1, members of the retinoblastoma family of transcriptional co-repressors, influence the energy status of cells and tissues(Bhattacharya et al., 2017; Dali-Youcef et al., 2007; De Sousa et al., 2014; Fajas, 2013; Jones et al., 2016; Petrov et al., 2016; Porras et al., 2017; Scime et al., 2005; Scime et al., 2010; Zacksenhaus et al., 2017). p107 is ubiquitously expressed in proliferating cells and its over expression has been shown to block cell cycle(Wirt and Sage, 2010). However, it is also implicated in controlling stem cell and progenitor metabolic fates(Bhattacharya et al., 2017) (De Sousa et al., 2014; Scime et al., 2005; Scime et al., 2010). Nonetheless, the fundamental mechanism that links p107 to metabolism and cell cycle has never been examined.

Key to understanding this relationship are the muscle resident myogenic stem cells (satellite cells) SCs, which are characterized by dynamic metabolic reprogramming during different stages of the differentiation process(Bhattacharya and Scime, 2020). They use predominately Oxphos in quiescence, but their committed progeny, the myogenic progenitor (MP) cells up-regulate glycolysis to support proliferation(Bhattacharya and Scime, 2020; Ryall et al., 2015). In this study, MPs were used to uncover a novel control mechanism of energy generation that showcases the interplay between glycolysis and Oxphos in regulating cell proliferation. Intriguingly, we found that p107 accomplishes this by controlling ATP generation capacity in the mitochondria through a Sirt1 dependent mechanism. Thus, our findings highlight a crucial role for p107 linking the regulation of mitochondrial Oxphos to proliferation dynamics in MPs that is likely to extend to other cell types.

Results

p107 is localized in the mitochondria of myogenic progenitor (MP) cells

By Western blotting cytoplasmic and nuclear cellular fractions, p107 was found in the cytoplasm of actively proliferating MP cell line c2c12 (c2MPs), as is the case in other cell types(Wirt and Sage, 2010) (**Fig. 1A**). Considering that emergent findings show that p107 can influence the metabolic state of progenitors(Porras et al., 2017), we assessed its potential metabolic role in the cytoplasm. As mitochondria are crucial in controlling metabolism, we assessed for the presence of p107 within this organelle. Intriguingly, Western blot analysis demonstrated that p107 was in the mitochondria fraction of the cytoplasm during proliferation, but almost absent when the cells were contact inhibited in confluent growth arrested cultures (**Fig. 1B**). To further assess for the presence of p107, we isolated various mitochondrial fractions utilizing hypotonic osmotic shock by varying sucrose concentrations(Lu et al., 2009). Mitochondrial fractionation showed that p107 was not located at the outer membrane nor within the soluble inner membrane fraction whose soluble proteins were relinquished by decreasing the buffer molarity (**Fig. 1C**). However, it was localized within the matrix where the protein constituents are unavailable to trypsin for digestion compared to the soluble inner membrane proteins such as Cox4, as well as p107 from the whole cell lysate control (**Fig. 1C**).

These results were corroborated by confocal microscopy and subsequent analysis of generated z-stacks that showed p107 and the mitochondrial protein Cox4 co-localize in c2MPs **(Fig. 1D)**. The specificity of immunocytochemistry was confirmed by immunofluorescence of p107 in p107 “knockout” c2MPs (p107KO c2MPs) generated by Crispr/Cas9 **(Fig. 1D & Suppl. Fig. 1A)**. Moreover, p107 and Cox4 fluorescence intensity peaks were matched on a line scanned RGB profile **(Fig. 1E)** and orthogonal projection showed co-localization in the XY, XZ, and YZ planes (**Fig 1F)**. The same assays were used to confirm these findings in proliferating primary wild type (Wt) MPs (prMPs) and p107 genetically deleted prMPs

(p107KO prMPs) isolated from Wt and p107KO mouse skeletal muscles, respectively **(Fig. 1G, 1H, 1I)**. In vivo, in a model of regenerating skeletal muscle caused by cardiotoxin injury, we also found p107 co-localized with Cox 4 in proliferating MPs, which express the myogenic stem cell marker Pax7 (**Fig. 1J, 1K & Suppl. Fig. 2).** Together, these data showcase that p107 localizes in the mitochondria of MPs from primary and muscle cell lines, suggesting that it might have an important mitochondrial function in the actively dividing cells.

p107 interacts at the mtDNA

To find the functional consequence of p107 mitochondrial matrix localization we assessed if it interacts at the mtDNA to repress mitochondrial gene expression similar to its role as a co-transcriptional repressor on nuclear promoters(Wirt and Sage, 2010). We evaluated this potential by performing quantitative chromatin immunoprecipitation (qChIP) analysis on the D-loop regulatory region of isolated mitochondria from c2MPs. qChIP revealed that p107 interacted at the mtDNA of growing c2MPs (**Fig. 2A**). It was negligible in growth arrested cells when p107 levels are deficient in the mitochondria and not detected in p107KO c2MPs (**Fig. 2A**).

p107 represses mtDNA encoded gene expression to regulate Oxphos capacity

We next appraised if p107 mtDNA promoter occupancy might repress mitochondrial encoded gene expression. For this we assessed 4 of 13 mitochondrial genes that are subunits of 4 of 5 ETC complexes. qPCR analysis showed that during proliferation when p107 is abundant in the mitochondria, there was significantly less expression of the mitochondrial encoded genes as compared to growth arrested cells (**Fig. 2B**). The importance of p107 to mitochondrial gene expression was confirmed with p107KO c2MPs and prMPs, which both exhibited significantly increased mitochondrial encoded gene expression in the genetically deleted cells compared to their controls (**Fig. 2C**). The increased mitochondrial gene expression and Oxphos in growth arrested and p107KO cells corresponded to augmented ETC

complex formation revealed by Western blot analysis of the relative protein levels of the 5 Oxphos complexes **(Fig. 2D).**

As mitochondrial gene expression is limiting for ETC complex formation, we used two methods to gauge if p107 promoter occupancy was associated with the capacity of mitochondria to generate ATP. First, using a luminescence assay, ATP generation potential capacity and rate were determined from isolated mitochondria, which were normalized to their protein content to exclude the potential contribution of mitochondria number. We found that the potential rate and capacity of ATP formation from isolated mitochondria of growth arrested cells and p107KO c2MPs were significantly higher than proliferating and control c2MPs, respectively **(Fig. 2E, 2F & Suppl. Table 1A)**, corresponding to the increase in mitochondrial gene expression profile and ETC complex formation **(Fig. 2B, 2C & 2D)**.

Second, we confirmed these results with live cell metabolic analysis using Seahorse, which showed that both growth arrested cells and p107KO c2MPs had significantly enhanced production of mitochondrial ATP generated compared to the proliferating and control c2MPs, respectively (Fig. 2G, 2H & Suppl. Fig. 3). As Oxphos is known to increase mitochondrial fusion causing elongation, we assessed a potential effect on mitochondrial morphology(Mishra et al., 2014; Mishra and Chan, 2016). Interestingly, we found that p107KO c2MPs had an elongated mitochondrial network (Fig. 2I) made up of mitochondria with significanly increased length and area (Fig. 2J). Together these data suggest that p107 has repressor activity when bound to the mtDNA promoter reducing the capacity to produce ETC complex subunits, which influences the mitochondria potential for ATP generation.

Glycolytic flux controls p107 mitochondrial function

The reliance of glycolysis versus Oxphos during the cell cycle can be driven by nutrient accessibility. Thus, we evaluated how nutrient availability influences p107 compartmentalization during proliferation. We assessed the effect of glucose metabolism on

p107 mitochondrial localization by growing c2MPs in stripped media with glucose as the sole nutrient. Western blot analysis of isolated mitochondria revealed that p107 translocation into mitochondria was glucose concentration dependent (**Fig. 3A)**. Its presence was negligible in mitochondria when cells were grown in 5.5mM glucose, but there was a significant increase of p107 localization in mitochondria at a higher glucose concentration (25mM). The increased level of mitochondrial p107 in c2MPs grown in higher glucose concentration corresponded to significantly increased mtDNA binding at the D-loop (**Fig. 3B**). This was associated with a significant decrease in mitochondrial encoded gene expression in both c2MPs and prMPs grown in high glucose concentration (**Fig. 3C & Suppl. Fig. 4**). However, increasing the glucose concentration in the stripped media had no effect on mitochondrial gene expression in the p107KO c2MPs and p107KO prMPs compared to their controls (**Fig. 3C & Suppl. Fig. 4**).

Importantly, our results also verified that changes in mitochondrial gene expression in MPs grown in varying glucose concentrations is not influenced by differences in mitochondrial biogenesis. By using qPCR, the gene expression of key markers of mitochondrial biogenesis *Pgc-1*α and *Mfn2* were not detected and there were no differences for expression of *Ant1* and *Nrf2* in c2MPs grown in 5.5mM compared to 25mM glucose (**Fig. 3D**). Moreover, the mtDNA to nuclear DNA ratio remained unchanged when grown in the different glucose concentrations, in contrast to MPs treated with the mitochondrial biogenesis activator AICAR (**Fig. 3E**). Together, these data show that mitochondrial gene expression might be mediated by glycolytic flux induced p107 mitochondrial gene repression and not merely a consequence of differences in mitochondrial biogenesis.

We next investigated if the reduction of mitochondrial gene expression with increased glucose availability influenced the potential mitochondrial ATP synthesis. In isolated mitochondria, we determined that there was a significant decrease in the potential rate and capacity of ATP generation when cells were grown in 25mM compared to 5.5mM glucose (**Fig.**

3F & Suppl. Table 1C). This corresponds to when p107 is in the mitochondria compared to low glucose when it is barely present. However, in the p107KO c2MPs, where mitochondrial gene expression was not influenced by glucose (**Fig. 3C**), the potential mitochondrial ATP rate and generation capacity also was unaffected by glucose **(Fig. 3G**). These data suggest that p107 is controlled by glucose metabolism to influence the potential mitochondrial energy production through regulation of the mitochondrial gene expression.

NAD^+/NADH regulates p107 mitochondrial function

As glucose metabolism affects the NAD^+/NADH redox balance, we determined if this might impact p107 mitochondrial localization and function. We found that c2MPs grown in 5.5mM compared to 25mM glucose in stripped media had significantly increased cytoplasmic NAD^+/NADH ratio (**Fig. 3H**). This suggests that the cytoplasmic NAD^+/NADH ratio might influence mitochondrial gene expression and ATP generation capacity via a p107 dependent mechanism.

We manipulated the cytoplasmic NAD^+/NADH energy flux in a glucose concentration independent manner to find the importance of the redox potential to p107 function. We added oxamate (ox) or dichloroacetic acid (DCA) to decrease the NAD^+/NADH ratio or grew cells in the presence of galactose instead of glucose, which increases NAD^+/NADH ratio (**Fig. 3I and Suppl. Fig 5A**). We also grew cells in varying amounts of glutamine in stripped media, which had no effect on the cytoplasmic NAD^+/NADH ratio (**Fig. 3I)**. As anticipated, Western blot analysis of c2MPs treated with ox and DCA showed significantly increased p107 levels in the mitochondria (**Fig. 3J and Suppl. Fig. 5B**). On the other hand, galactose treated cells had significantly less p107 in the mitochondria compared to untreated controls and cells treated with glutamine showed no difference in the level of p107 mitochondrial localization (**Fig. 3J**). These results suggest that p107 mitochondrial localization is based on the cytoplasmic NAD^+/NADH ratio. Mitochondrial gene expression levels with the different treatments

corresponded with p107 mitochondrial localization established by the cytoplasmic NAD^+/NADH ratio (**Fig. 3K and Suppl. Fig. 5C**). Indeed, significantly higher mitochondrial gene expression levels were observed with higher cytoplasmic NAD^+/NADH when cells were grown with galactose compared to glucose, whereas significantly lower mitochondrial gene expression was evident when cells were treated with ox and DCA that caused decreased cytoplasmic NAD^+/NADH (**Fig. 3K and Suppl. Fig. 5C**). No significant gene expression changes were present when cells were grown solely with varying amounts of glutamine, except *Nd6,* which is the only mitochondrial gene expressed from the L-strand of mtDNA (**Fig. 3K**). Together, these results show that p107 acts indirectly as an energy sensor of the cytoplasmic NAD^+/NADH ratio that might influence the potential ATP produced from the mitochondria, as a consequence of regulating mitochondrial gene expression.

Sirt1 directly regulates p107 mitochondrial function

As the NAD^+ dependent Sirt1 deacetylase is an energy sensor of the NAD^+/NADH ratio, we evaluated if it potentially regulates p107. Importantly, reciprocal Immunoprecipitation/Western analysis on c2MP lysates for endogenous p107 and Sirt1 showed that they directly interacted (**Fig. 4A)**. No interactions were apparent in p107KO and Sirt1genetically deleted (Sirt1KO) c2MPs obtained by Crispr/Cas9 (**Fig. 4A and Suppl Fig. 1B**).

We next assessed if Sirt1 activity affected p107 mitochondrial function. Unlike c2MPs grown in 5.5mM glucose that exhibit relocation of p107 from the mitochondria, Sirt1KO cells did not alter p107 mitochondrial localization **(Fig. 4B & 3A).** This resulted in significantly decreased mtDNA encoded gene expression for Sirt1KO cells grown in 5.5mM glucose compared to controls and no differences between Sirt1KO cells grown in 5.5mM or 25mM glucose **(Fig. 4C)**. The decreased mitochondrial gene expression in Sirt1KO cells grown in 5.5mM glucose corresponded with a reduced mitochondrial ATP generation rate and capacity

compared to control cells (**Fig. 4D & Suppl. Table 1D)**. There were no differences in ATP generation rate or capacity between Sirt1KO cells grown in 5.5mM or 25mM glucose **(Suppl. Fig. 6**).

We next determined if Sirt1 activity is necessary for p107 mitochondrial function. Inhibition of Sirt1 activity by nicotinamide (nam) increased p107 mitochondrial localization (**Fig. 4E**) that was concomitant with increased mtDNA promoter interaction (**Fig. 4F**). This was associated with decreased mitochondrial gene expression, whereas nam treatment of p107KO and Sirt1KO c2MPs had no effect on the mitochondrial gene expression (**Fig. 4G**). This suggests that Sirt1 control of mitochondrial gene expression is dependent on p107. As expected, both the potential ATP generation rate and capacity of isolated mitochondria were reduced with Sirt1 attenuated activity (**Fig. 4H & Suppl. Table 1E**). On the contrary, Sirt1KO c2MPs showed no difference in ATP generation capacity and rate, and no changes in mitochondrial gene expression profile (**Fig. 4I**). Moreover, the reduction of Oxphos capacity by attenuated Sirt1 activity was not due to an apparent decrease in mitochondrial biogenesis, as nam treatment did not influence the mtDNA/nDNA ratio (**Fig. 4J)**.

To confirm these results, we also used resveratrol (res) at low and high doses that indirectly activate and inhibit Sirt1 activity, respectively. c2MPs grown in a low concentration of res (10μM), had the opposite effect to nam for p107 localization and function. Treatment of c2MPs with this concentration of res decreased p107 within the mitochondria (**Fig. 4K)**. The activation of Sirt1 also reduced p107 mtDNA promoter interaction and enhanced the mitochondrial gene expression (**Fig. 4L & 4M**), which corresponded to an increased ATP synthesis rate and capacity of isolated mitochondria (**Fig. 4N & Suppl. Table 1F**). No differences in ATP generation rate and capacity were observed in Sirt1KO c2MPs, which was anticipated with a non-significant consequence on mitochondrial gene expression (**Fig. 4M & 4O**). When Sirt1 activity was repressed by high doses of res, p107 was localized in the

mitochondria and gene expression along with ATP generation rate and capacity were significantly decreased (**Suppl. Fig. 7 & Suppl. Table 1G**).

We further assessed the role of Sirt1 activity on p107 localization by overexpressing c2MPs with Ha tagged p107 in the presence of full length Sirt1 (Sirt1fl) or dominant negative Sirt1(Sirt1dn). Similar to Sirt1KO cells, Sirt1dn had no effect on preventing p107 mitochondria localization when grown in 5.5mM glucose as opposed to Sirt1fl **(Compare Fig. 4B & Suppl. Fig. 8).** As expected, the Sirt1fl overexpression did not alter p107 localization in cells grown in 25 mM glucose (**Suppl. Fig. 9).** Also, there was significantly less mitochondrial encoded gene expression in Sirt1dn cells grown in 5.5mM glucose compared to Sirt1fl **(Compare Fig 4C & Suppl Fig. 10)**. Together, these results suggest that p107 is influenced directly by Sirt1 activity to localise within the cytoplasm, de-repressing mitochondrial gene expression and hence increasing ATP generation capacity.

p107 directs cell cycle rate through management of Oxphos generation

We next considered how this metabolic role for p107 might influence MP behaviour in vivo by assessing skeletal muscle regeneration caused by cardiotoxin injury (**Fig. 5A & Suppl. Fig. 11**). Immunofluorescence of MP marker MyoD and proliferation marker bromodeoxyuridine (Brdu), revealed significantly more proliferating MPs in p107KO tibialis anterior (TA) muscle compared to wild type regenerating muscle, 2 days post cardiotoxin injury (**Fig. 5A**).

We confirmed that the proliferative differences in the p107 genetically deleted mice compared to wild type littermates were cell autonomous by considering control and p107KO c2MPs. By counting cells over several days and performing flow cytometry cell cycle analysis, we found p107KO c2MPs had almost twice the cell cycle rate, with significantly increased cell numbers in S-phase compared to control c2MPs, as had been previously shown with p107KO prMPs (LeCouter et al., 1998) (**Fig. 5B & 5C**). Contrarily, Sirt1KO cells that had increased

levels of p107 in the mitochondria (**Fig. 4B**) exhibited significantly decelerated cell cycle progression with significantly fewer cells in S-phase compared to controls **(Fig. 5C)**. We assessed if the mitochondrial function of p107 was essential to the cell cycle rate reduction, by restoring p107 mitochondrial localization in p107KO cells. This was accomplished by over expressing p107fl or p107 containing a mitochondrial localization sequence (p107mls) (**Fig. 5D & Suppl. Fig. 12A**). Restoring p107 to the genetically deleted cells significantly inhibited cell cycle progression by blocking cells in G1 phase of the cell cycle, which corresponded to reduced mitochondrial gene expression (**Fig. 5E & Suppl. Fig. 12B**). This suggests that p107 might direct the cell cycle rate through management of Oxphos generation.

We tested this possibility by using live cell metabolic imaging with Seahorse, which showed that the augmented cell cycle rate in p107KO cells compared to controls corresponded to a significant increase rate of ATP generation from Oxphos and glycolysis, including an increase in the mitochondrial to glycolytic ATP production rate ratio (**Fig. 5F)**. In contrast, live cell metabolic imaging by Seahorse showed that p107KO c2MPs that over-expressed p107fl or p107mls, which is directed to the mitochondria, resulted in significant attenuation of ATP generation capacity **(Suppl. Fig. 13)**.

We next appraised if modulation of p107 mitochondrial function to control ATP production might influence MP proliferation. For this, the cytoplasmic NAD^+/NADH ratio was manipulated with addition of ox (**Fig. 3I**). As ox inhibits Ldha, it results in glycolytic flux relying almost entirely on NAD^+ generated by Oxphos. It also provides increased NADH, which augmented p107 mitochondrial localization and decreased mtDNA gene expression (**Fig. 3J, 3k & 5G**). However, ox did not affect mitochondrial gene expression in p107KO cells (**Fig. 5G**). Moreover, Western blotting revealed that ox treatment also decreased ETC complex levels in c2MPs but showed no change in p107KO c2MPs (**Fig. 5H**).

Live metabolic imaging of c2MPs demonstrated that the reduction in ETC complexes with ox was associated with a significant decrease in ATP generation from Oxphos as well as glycolysis (**Fig. 5I and Suppl. Fig. 14**). The reduced ATP production was coupled to a significant decrease in cell growth and proliferation rate (**Fig. 5J & 5K**) as well as the cell cycle rate and S-phase (**Fig 5L**). However, ox treatment of p107KO c2MPs did not alter ATP levels, and the cell cycle rate (**Fig. 5I, 5J, 5K & 5L**). Taken together, these results suggest that Oxphos regulation by p107 controls c2MP proliferative rates.

We confirmed these findings in vivo by treatment of mice with ox during the regeneration process. Wild type mice treated with ox showed significantly fewer proliferating $MyoD^{+}Brdu^{+}$ MPs compared to control untreated mice (**Fig. 5M, 5N & Suppl. Fig. 15**). In contrast, the muscles from p107KO mice treated or untreated with ox showed no difference in proliferating MPs (**Fig. 5M, 5N and Suppl. Fig. 15**).

Collectively, these results suggest that p107 mitochondrial function controls cell cycle rate by regulating ETC complex formation in a Sirt1 dependent manner (**Suppl. Fig. 16**).

Discussion

Our results for the first time support an unanticipated mitochondrial function for p107 as a regulator of ATP generation. We used a series of complimentary approaches that underscore p107 operation within the mitochondria as a transcriptional co-repressor. Biochemical mitochondrial fractionation showed that it is located in the matrix and interacts at the D-loop promoter of mtDNA to repress gene expression. By controlling gene expression in this manner, we found that p107 directly impacted the Oxphos capacity of MP cells and restricted their proliferation rate. Accordingly, these findings showcase that p107 arbitrates cell cycle rate through metabolic control. Indeed, p107 mitochondrial function is controlled by the cellular redox status and in particular the energy sensor Sirt1 an NAD^+ dependent deacetylase. Intriguingly, as p107 is almost always shown to be expressed only in proliferating cells, the p107-Sirt1 pathway in MPs is possibly a universal cell mechanism utilized during division.

For many years, assigning a functional role for p107 has been ambiguous, unlike family member Rb that is a bona fide G1 phase restriction check point factor(Wirt and Sage, 2010). In this study we found that p107 acts as a metabolic checkpoint molecule for cellular energy status, placing it within the pantheon of other well-known nutrient sensing cell growth checkpoint molecules(Foster et al., 2010). During cell division, it is unclear how glycolysis and Oxphos collectively operate to regulate the yield of ATP. Our data show a major rationale for the ubiquitous expression of p107 in proliferating cells as part of a mechanism involved in this interplay. Our results highlight that p107 influences ATP production in the mitochondria based on the energy generated in the cytoplasm, in a Sirt1 dependent manner. The lowering of the NAD^+/NADH ratio by a higher glycolytic flux was concomitant with a decreased capacity to generate ATP from Oxphos. We believe this is in part due to increasing levels of p107 interacting at the mtDNA where it represses gene expression to limit ETC complex formation. At this time, it is not known how p107 is shuttled across the outer and inner mitochondrial

membranes. It might be a result of post-translational modification by acetylation and/or phosphorylation.

The role of p107 in repressing mtDNA transcription might ensure that ATP levels remain compatible with the demands of the proliferating cells and might also help steer the TCA cycle away from producing reducing equivalents in favour of biomass production(Vander Heiden and DeBerardinis, 2017). Notably, p107 is found to relocate from the cytoplasm to nucleus at late G1 or G1/S phase(Lindeman et al., 1997; Muller et al., 1997; Rodier et al., 2005; Verona et al., 1997; Zini et al., 2001). This is when a glycolytic to Oxphos switch occurs and when it silences Ldha and Pdk2 gene expression on nuclear promoters to further increase Oxphos capacity as shown in adipocyte progenitors(Porras et al., 2017). Thus, we propose that p107 dynamically modulates cell metabolism during the cell cycle through promoter repression in two different organelles. Through inhibiting Oxphos in G1, dependent on the nutrient load, and increasing Oxphos in S phase p107 is able to exert dual influences on cell cycle progression.

The high rate of ATP generated by Oxphos and glycolysis in p107KO MPs can explain the accelerated cell cycle rate. The higher proliferative rate is also characteristic of p107KO MEFs and primary MPs(LeCouter et al., 1998) and was evidenced in the significantly greater number of proliferating MPs within regenerating p107KO skeletal muscle. Conversely, if p107 function is dysregulated and forced to remain in the mitochondria, the reduced ATP generation capacity alarmingly decreases cell cycle efficiency. Thus, the decreased proliferative capacity of p107 over expressing cells found in many reports might now be attributed to a mitochondrial role in repressing mitochondrial gene expression, which is required for G1 cell cycle progression. Indeed, over expression of p107 can inhibit cell proliferation and arrest cell cycle at G1 in many cell types(Leng et al., 2002; Wirt and Sage, 2010; Zhu et al., 1993) and delay the G1 to S phase entry in rat fibroblast cell lines(Rodier et al., 2005).

Our data strongly support the concept that the NAD^+/NADH ratio controls p107 function through Sirt1, which is activated by NAD^+. Moreover, we and others have shown that Sirt1 regulation of SC and MP cell cycle parallels p107 mitochondrial control of proliferation. Indeed, Sirt1 has been shown to promote MP proliferation(Rathbone et al., 2009; Wang et al., 2016), which corresponds to p107 relocation from the mitochondria. Consistent with this idea, mice with activated Sirt1 (by caloric restriction or by NAD^+ repletion) exhibited greater SC self-renewal and more proliferative MPs(Cerletti et al., 2012; Fulco et al., 2008; Ryall et al., 2015; Zhang et al., 2016). Conversely, primary activated SCs isolated from Sirt1KO, as well as conditional Sirt1KO, that would increase p107 mitochondrial localization and repress mtDNA gene expression, showed significantly lowered cell cycle as measured by the incorporation of nucleotide base analogs into DNA(Myers et al., 2019; Tang and Rando, 2014). Though the use of Sirt1KO cells confirmed that p107 functions through a Sirt1 dependent mechanism, it is unlikely that the functional interaction between p107 and Sirt1 is maintained during myogenic differentiation, as Sirt1 has a non-metabolic role during differentiation(Fulco et al., 2003; Ryall et al., 2015). Nonetheless, these findings set the stage for future evaluation of the mitochondrial function of p107 during SC activation, self-renewal and commitment.

In summary, our findings establish that a cell cycle regulator, p107, functions as a key and fundamental component of the cellular metabolism network during cell division. Indeed, it directly manipulates the energy generation capacity of mitochondria by indirectly sensing the glycolytic energy production through Sirt1. These results provide a conceptual advance for how proliferating cells regulate energy generation through the interplay between glycolysis and Oxphos. Importantly because of the ubiquitous p107 protein expression in most dividing cells, the findings identify a potential universal cellular mechanism with immense implications for studies on cancer cell proliferation and stem cell fate decisions.

Materials and Methods

The c2c12 myogenic progenitor cell line (c2MP) was purchased from the American Tissue Type Culture (ATTC) and grown in Dulbecco's Modified Eagle Medium (DMEM) (Wisent) containing 25mM glucose supplemented with 10% fetal bovine serum (FBS) and 1% penicillin streptomycin. Primary myogenic progenitor cells (prMPs) were grown on rat tail collagen I (ThermoFisher Scientific) coated dishes containing in Ham's F10 Nutrient Mix Media (ThermoFisher Scientific) supplemented with 20% FBS, 1% penicillin streptomycin and 2.5ng/ml bFGF (PeproTech).

For the nutrient specific experiments, c2MPs or prMPs were grown in stripped DMEM with 10% FBS and 1% penicillin streptomycin for 20 hours supplemented with 1mM, 5.5mM or 25mM glucose; or 4mM or 20mM glutamine; or 4mM glutamine with 25mM glucose or 10mM galactose for 6 hours. For drug specific treatment, c2MPs were grown in DMEM with 10% FBS, 1% penicillin streptomycin, supplemented with 2.5mM oxamate (ox) for 40 hours. For Sirt1 inhibition, cells were grown in stripped DMEM with 10% FBS and 1% penicillin streptomycin and 5.5mM glucose with or without 10mM nicotinamide (nam) for 20 hours. For Sirt1 activation, cells were grown in DMEM with 10% FBS, 1% penicillin streptomycin with or without 10μM resveratrol (res) and for inactivation with 25μM res for 18 hours.

Primary myogenic progenitor cell (prMP) isolation

All animal experiments were performed following the guidelines approved by the Animal Care Committee of York University. For derivation of prMPs and tissue immunofluorescence wild type and p107KO mice were from M. Rudnicki(LeCouter et al., 1998) maintained on a mixed (NMRI, C57/Bl6, FVB/N) background(Chen et al., 2004). Extensor digitorum longus muscles of 3-month aged mice were dissected from tendon to tendon and digested in filter sterilized 0.2% type 1 collagenase (Sigma Aldrich) in serum free DMEM for 30 minutes. Upon

unravelling, it was transferred to a pre-warmed petri dish containing DMEM (Wisent) with 1% penicillin, streptomycin. The muscle was then flushed gently with the media until it released the fibers with an intermittent incubation at 37°C every 5 minutes. After 30 minutes, individual fibers were transferred into 24 well rat tail collagen I (ThermoFisher Scientific) coated tissue culture plate containing pre-warmed Ham's F10 Nutrient Mix Media (ThermoFisher Scientific) with 20% FBS, 1% penicillin, streptomycin and 2.5ng/ml bFGF (PeproTech). After 3 days, the fibers were transferred to collagen coated Ham's F10 Nutrient Mix Media with 20% FBS, 1% penicillin, streptomycin and 2.5ng/ml bFGF (PeproTech). The media was changed every alternate day, until the fibers generated prMPs that were collected by trypsinization and passaging onto collagen coated plates to remove live fibers.

Cloning

The p107mls expression plasmid that expresses p107 only in the mitochondria was made by cloning full length p107 into the pCMV6-OCT-HA-eGFP expression plasmid vector(Newman et al., 2016) that contains a mitochondrial localization signal. We used the following forward 5'-CACCAATTGATGTTCGAGGACAAGCCCCAC-3' and reverse 5'-CACAAGCTTTTAATGATTTGCTCTTTCACT-3' primer sets that contain the restriction sites Mfe1 and HindIII, respectively, to amplify full a length p107 insert from a p107 Ha tagged plasmid(Iwahori et al., 2017). The restriction enzyme digested full length p107 insert was then ligated to an EcoRI/HindIII digest of pCMV6-OCT-HA-eGFP, which removed the HA-eGFP sequences but retained the n-terminal mitochondrial localization signal (OCT).

Transfections

The calcium chloride method was used for transfections, whereby a mixture containing a total of 10μg of plasmid DNA, 125mM $CaCl_2$ and H_2O were added dropwise to HEBS buffer (274mM NaCl, 10mM KCl, 1.4mM Na_2HPO_4, 15mM D-glucose and 42mM HEPES), incubated at room temperature for 1 hour and then added to 1×10^5 cells that had been passaged

on the previous day. 18 hours post transfection, fresh DMEM containing 25mM glucose supplemented with 10% fetal bovine serum (FBS) and 1% penicillin streptomycin was added, and the cells used the next day. For overexpression studies, at least 4 different p107KO c2MPs were transfected as above with GFP mitochondrial localization empty vector pCMV6-OCT-HA-eGFP(Newman et al., 2016), p107fl expressing full length p107 tagged HA, and p107mls expressing full length p107, which is directed to the mitochondria. For Sirt1 overexpression experiments, c2MPs were transfected with p107fl alone expressing full length p107 tagged HA or with full length (Sirt1fl) or dominant negative (Sirt1dn) Sirt1(Boily et al., 2009).

p107KO and SirtKO cell line derivation

Crispr/Cas9 was used to generate p107 and Sirt1 genetically deleted c2MP (p107KO and SirtKO) cell lines. For p107KO c2MPs, c2c12 cells were simultaneously transfected with 3 pLenti-U6-sgRNA-SFFV-Cas9-2A-Puro plasmids each containing a different sgRNA to target p107 sequences 110 CGTGAAGTCATCCAGGGCTT, 156 GGGAGAAGTTATACACTGGC and 350 AGTTTCGTGAGCGGATAGAA (Applied Biological Materials), and for Sirt1KO with 2 Double Nickase plasmids each containing a different sgRNA to target sequences 148 CGGACGAGCCGCTCCGCAAG and 110 CCATGGCGGCCGCCGCGGAA (Santa Cruz Biotechnology). Following 18 hours of incubation, the media was changed for 6 hours and then passaged into 96 well tissue culture plates. On the next day, the media was aspirated and replenished with DMEM containing 2mg/ml puromycin for antibiotic selection. Following, the media was changed every 2 days until cell clones were visible. Any surviving clones was grown and tested by Western blotting. For control cells, c2MPs cells were transfected by empty pLenti-U6-sgRNA-SFFV-Cas9-2A-Puro (Applied Biological Materials) and selected as above.

Mitochondrial, nuclear and cytosolic isolation

For nuclear and cytoplasmic isolation, at least cells were pelleted, washed in PBS, dissolved in 500µl of cytoplasmic buffer (10mM Tris pH 7.4, 10mM NaCl, 3mM $MgCl_2$, 0.5% NP-40 and protease inhibitors) and incubated on ice for 5 minutes followed by rocking on ice for 5 minutes. After centrifugation at 2500g for 5 minutes at 4ºC, the supernatant was stored as the "cytoplasmic fraction". The cell pellet that represents the "nuclear fraction" was then washed 8 times with the cytoplasmic buffer and lysed with nuclear lysis buffer containing 50mM Tris pH 7.4, 5mM $MgCl_2$, 0.1mM EDTA, 1mM dithiothreitol (DTT), 40% (wt/vol) glycerol and 0.15 unit/µl benzonase (Novagen).

For mitochondrial and cytosolic isolation, at least 1 million cells were washed in PBS, pelleted, dissolved in 5 times the packed volume with isolation buffer (0.25M Sucrose, 0.1% BSA, 0.2mM EDTA, 10mM HEPES, pH 7.4; with 1mg/ml of each pepstatin, leupeptin and aprotinin protease inhibitors), transferred into a prechilled Dounce homogenizer and homogenized loose (5-6 times) and tight (5-6 times) on ice. The homogenate was transferred into an eppendorf tube and centrifuged at 1000g at 4ºC for 10 minutes. The supernatant was then centrifuged at 14000g for 15 min at 4ºC and the resulting supernatant was saved as "cytosolic fraction". The pellet representing the "mitochondrial fraction" was washed twice and dissolved in 50µl of isolation buffer. The mitochondria were lysed by repeated freeze-thaw cycles (3 times each) on dry ice.

Mitochondria fractionation

Mitochondrial fractions were isolated using a hypotonic osmotic shock approach(Lu et al., 2009). For this, cells were collected by centrifugation at 1500rpm and the cell pellet resuspended in STE buffer (250mM sucrose, 5mM Tris pH 7.4 and 1mM EGTA), Dounce homogenized and centrifuged at 1000g for 3 mins to remove cell debris. The supernatant was then centrifuged at 10,000g for 10 mins to isolate pelleted mitochondria. The mitochondria

were resuspended in STE buffer containing 250mM sucrose and centrifuged at 16000g for 10 minutes to isolate matrix (M) and inner membrane (IM) proteins and the outer membrane (OM) proteins in the pellet and supernatant, respectively. To obtain a pure mitochondria matrix protein (M) fraction the isolated mitochondria were resuspended in hypotonic STE buffer containing 25mM sucrose and centrifuged at 16000g for 10 mins. After centrifugation, the soluble inner membrane (IMS) and outer membrane (OM) protein fractions were present in the supernatant and the matrix protein fraction (M) in the pellet. To demonstrate mitochondria matrix veracity, 50μg/ml porcine trypsin (Promega) was added for 30 mins followed by 20μg/ml trypsin inhibitor aprotinin (Roche) for 10 minutes before centrifugation at 16000g for 10 mins. Only fractions containing M proteins were unavailable for trypsin digestion. As a control whole cell treatment of c2MPs with both buffers showed that trypsin treatment can digest p107.

Western blot analysis

For Western blot analysis, cells were lysed in RIPA buffer (0.5% NP-40, 0.1% sodium deoxycholate, 150mM NaCl, 50mM Tris-Cl pH 7.5, 5mM EDTA) or mitochondrial isolation buffer (0.25M sucrose, 0.1% BSA, 0.2mM EDTA, 10mM HEPES, pH 7.4) containing protease inhibitors (1mg/ml of each of pepstatin, aprotinin and leupeptin). Protein lysates were loaded on gradient gels (6-15%) or 7.5% gels. Proteins were transferred using a wet transfer method onto a 0.45μm pore sized polyvinylidene difluoride membrane (Santa Cruz Biotechnology) at 4ºC for 80 minutes at 100V. The membranes were blocked for an hour at room temperature in 5% non-fat milk in Tris-Buffered saline (TBS-150mM NaCl and 50mM Tris base) containing 0.1% Tween-20 (TBST). The membranes were probed overnight at 4ºC with primary antibodies (listed below) diluted in 5% non-fat milk or 1% BSA in TBST. The membranes were then washed three times with TBST and secondary antibodies conjugated with horseradish peroxidase diluted in 5% non-fat milk in TBST were added for an hour at room

temperature with gentle rocking. The membranes were then washed 3 times with TBST and visualized with chemiluminescence on photographic films. Protein levels were evaluated by densitometry using Image J software.

Primary antibodies used

α-tubulin (66031, Proteintech); Cox4 (ab16056, Abcam) and Total OXPHOS rodent WB antibody cocktail (Abcam); p107-C18, p107-SD9, histone H3-C16, Sirt1-B7, IgG-D7, Ha-tag-F7, Brdu-MoBU-1, Pax-7 (EE8) (Santa Cruz Biotech); MyoD (Novus Biologicals) and Sirt1-D1D7 (Cell Signaling).

Co-immunoprecipitation

For Immunoprecipitation (IP), protein lysates were pre-cleared with 50µl protein A/G plus agarose beads (Santa Cruz Biotechnology) by rocking at 4ºC for an hour. The sample was centrifuged at 15000 rpm for a minute. Fresh protein A/G agarose beads along with 5µg of p107-C18, Sirt1-B7 or IgG-D7 antibody (Santa Cruz Biotechnology) antibody were added to the supernatant and rocked overnight at 4ºC. The next day the pellets were washed 3 times with wash buffer (50mM HEPES pH 7.0, 250mM NaCl and 0.1% Np-40) and loaded onto polyacrylamide gels and Western blotted for p107-SD9 (Santa Cruz Biotechnology) or Sirt1-D1D7 (Cell Signaling). Inputs represent 10% of lysates that were immunoprecipitated.

qPCR

RNA was isolated using Qiazol reagent (Qiagen) and concentration was determined by NanoDrop 2000 (ThermoFisher Scientific). qPCR experiments were performed according to the MIQE (Minimum Information for Publication of Quantitative Real-Time PCR Experiments) guidelines (Bustin et al., 2009). The optical density (OD) of RNA was measured using the NanoDrop 2000 (Thermo Fisher Scientific), RNA purity was inferred by the A260/280 ratio (~1.80 is pure). 1µg of RNA was reverse transcribed into cDNA using the All-in-One cDNA Synthesis SuperMix (Bimake) and the cDNA used for qPCR. qPCR assays were

performed on Light cycler 96 (Roche) using SYBR green Fast qPCR Master mix (Bimake) with appropriate primer sets and Rplp0 (36B4) as a normalization control was used (**Suppl. Table 2**). Relative expression of cDNAs was determined with 36B4 as the internal control using the ΔΔCt method. For fold change, the ΔΔCt was normalized to the control. Student t-tests, one-way or two-way Anova and Tukey post hoc tests were used for comparison and to obtain statistics.

Mitochondrial and nuclear DNA content

To obtain the mitochondrial to nuclear DNA ratio (mtDNA/nDNA), cells grown on a 6cm tissue culture plate were untreated or treated with 1mM 5-aminoimidazole-4-carboxamide-1-β-D-ribofuranoside (aicar) (Toronto Research Chemicals) in presence of 5.5mM or 25mM glucose, with or without 10mM Nam or 10μM resveratrol for 24 hours. The cells were washed in PBS and lysed with 600μl of lysis buffer containing 100mM NaCl, 10mM EDTA, 0.5% SDS solution, 20mM Tris HCl; pH 7.4 and 6μl of 1μg/μl proteinase k (ThermoFisher Scientific). Following incubation at 55ºC for 3 hours, 100μg/ml RNase A (ThermoFisher Scientific) was added at 37ºC for 30 minutes. After, 250μl of 7.5M ammonium acetate and 600μl of isopropanol were added, the cells were centrifuged at 15000g for 10 minutes at 4ºC. The supernatant was discarded and the pellet containing mitochondrial and nuclear DNA was washed with 70% ethanol and resuspended in Tris EDTA buffer (10mM Tris HCl pH 7.4, 1mM EDTA). qPCR assays were performed on 10ng DNA with primer sets to Mt-Co1 and H19 (**Suppl. Table 2**) representing total mitochondrial and nuclear DNA content, respectively. Ct values were obtained and the ratio mtDNA:nDNA were determined by the formula: nDNA Ct-mtDNA Ct.

Quantitative chromatin immunoprecipitation assay (qChIP)

qChIP was performed on mitochondrial lysates containing only mitochondrial DNA. Mitochondrial fractions were collected as described above, washed twice in PBS by centrifugation at 14000g for 15 minutes at 4°C, resuspended in 200µl of PBS containing 1% formaldehyde and rocked at room temperature for 30 minutes to fix the cells. The fixation reaction was quenched by adding 125mM of glycine in PBS and rocked for 5 minutes at room temperature. The fixed pellet was washed twice in PBS containing 100mM NaF and 1mM Na_3VO_4 by centrifuging at 14000g for 5 minutes at 4°C. The pellet was the resuspended in 500µl of ChIP lysis buffer (40mM Tris, pH 8.0, 1% Triton X-100, 4mM EDTA, 300mM NaCl) and sonicated at 24% amplitude, 15 seconds on, 15 second off for 3 cycles (Model 120 Sonic Dismembrator, ThermoFisher Scientific). Following sonication, the samples were centrifuged at 13000 rpm for 10 minutes at 4°C and the supernatant was transferred to a new tube containing 100µl of dilution buffer 1 (40mM Tris, pH 8.0, 4mM EDTA) from which the input controls were removed before 150 µl of dilution buffer 2 (40mM Tris, pH 8.0, 0.5% Triton X-100, 4mM EDTA, 150mM NaCl) was added. To preclear, 50µl of protein A/G agarose beads (Santa Cruz Biotechnology) was added and rocked for 90 minutes at 4°C. The beads were then pelleted and discarded, and to the supernatant was added 5µg of p107 antibody (p107- C-18) (Santa Cruz Biotechnology) or IgG antibody (IgG-D-7) (Santa Cruz Biotechnology). This was rocked overnight at 4°C and on the following day, 50µl of protein A/G agarose beads were added and rocked for 90 minutes at 4°C. The beads were collected by centrifugation and were washed sequentially with 5 minutes rocking at 4°C before centrifugation by adding the following: low salt complex wash buffer (0.1% SDS, 1% Triton X-100, 2mM EDTA, 20mM Tris HCl, pH 8.0, 150mM NaCl), high salt complex wash buffer (0.1% SDS, 1% Triton X-100, 2mM EDTA, 20mM Tris HCl, pH 8.0, 500mM NaCl), LiCl wash buffer (0.25M LiCl, 1% NP-

40, 1% deoxycholic acid, 1mM EDTA, 10mM Tris, pH 8.0) and 2 washes with TE buffer (10mM Tris HCl, pH 8.0, 1mM EDTA). After the last wash, the mtDNA-protein complexes were isolated by resuspending the beads in 250µl of elution buffer (1% SDS, 0.1M $NaHCO_3$), vortexing, rocking for 15 minutes at room temperature and centrifuging at 2000 rpm in a microcentrifuge for 2 minutes. The supernatant was transferred to a clean tube and to the remaining beads another 250µl of elution buffer was added and the isolation step repeated. For isolation of mtDNA fragments, to the 500µl of mtDNA-protein complexes in elution buffer, 20µl of 5M NaCl was added and incubated at 65°C overnight. The next day, the DNA was isolated using DNA purification kit (Thermo Fisher Scientific), and the concentration determined using the NanoDrop 2000 (ThermoFisher Scientific). Relative occupancy was determined by amplifying isolated DNA fragments using the D-loop primer sets (**Suppl. Table 2**) analyzed using the ΔΔCt method and the fold changes were normalized to IgG ΔΔCt values.

NAD^+/NADH assay

Cells growing in 6cm tissue culture plates were washed with PBS and scraped into 500µl of 0.5M perchloric acid, vortexed and freeze-thawed on dry ice three times. The cells were then centrifuged at 4°C for 5 minutes at 7,000 rpm in a microfuge and 100µl of 2.2M $KHCO_3$ was added to the supernatant on ice. This was again centrifuged at 7,000 rpm for 15 minutes at 4°C and the supernatant was collected to be analyzed. For the lactate assay; 20µl of the supernatant, 258µl of lactate buffer (1M glycine, 500mM hydrazine sulfate, 5mM EDTA), 20µl of 25mM β-nicotinamide-adenine dinucleotide (NAD) (Roche) and 2µl of porcine heart lactate dehydrogenase (Ldh) (Sigma-Aldrich) were added to each well of an assay plate. For the pyruvate assay; 20µl of the supernatant, 218µl of pyruvate buffer (1.5M Tris, pH 8), 180µl of 6µM β-nicotinamide-adenine dinucleotide, reduced (NADH) (Roche) and 2µl of rabbit skeletal muscle LDH (Sigma-Aldrich) were added for each well. The assay plates were then read by a

microplate reader (Glomax, Promega) with excitation at 340nm and emission peak at 450nm and the concentration values were attained by comparing to standard curves. The standard curves were made with NADH (Roche) at 0, 2, 3, 4, 5, 6, 7, and 10mM in lactate buffer for the lactate assay and in pyruvate buffer for the pyruvate assay. Estimation of free NAD^+/NADH in cells was based on lactate/pyruvate (pyruvate + NADH + H^+ = lactate + NAD^+). The results were normalized to control samples and graphed.

ATP generation capacity and rate assay

The ATP generation capacity assay is based on the requirement of luciferase for ATP in producing light from the reaction:

$$\text{Luciferin} + \text{ATP} + O_2 \xrightarrow{\text{Luciferase}} \text{Oxyluciferin} + \text{AMP} + \text{Pyrophosphate} + CO_2 + \text{Light}$$

It was measured from mitochondrial fractions by using the ATP determination kit (ThermoFisher Scientific). In each well of a 96 well assay plate, 10µl of the isolated mitochondria was added to 4µl of 100mM ADP and 86 µl of reaction mix (1.78µl ddH_2O, 100µl of 20X reaction buffer, 20µl of 0.1M DTT, 100µl of 10mM D-luciferin and 0.5µl firefly luciferase from a 5mg/mL stock solution, all supplied by the kit manufacturer). The plate was then read over a period of 15 minutes every 1 minute for emission peak at 560 nm by a microplate reader (Glomax, Promega). The amount of ATP generated was normalized to the protein content of the mitochondrial fractions determined by Bradford Assay Kit (Biobasic) and graphed over time. The ATP generation rate was calculated from the slope of the graph of ATP that was produced over time up to the point where its production reached a steady state.

Immunocytochemistry and confocal imaging

For confocal microscopy, cells were grown on Nunc Lab-Tek™ II chambered tissue culture plates (ThermoFisher Scientific), fixed for 5 minutes with 95% methanol and permeabilized

for 30 minutes at 4ºC with blocking buffer (3% BSA and 0.1% saponin in PBS). Cells were then incubated with primary antibody p107-SD9 or HA-tag-F7 (Santa Cruz Biotechnology) in 1:100 dilution in blocking buffer for 1 hour. After 3 washes with 0.05% saponin in PBS (SP), cells were incubated with secondary antibody donkey anti-mouse IgG NL493-conjugated (R and D Systems) at a 1:200 dilution in blocking buffer. Cells were then washed 3 times in SP and re-incubated with primary antibody Cox4 (Abcam) at a 1:100 dilution in blocking buffer for 1 hour. After 3 washes in SP, cells were incubated with secondary antibody goat anti rabbit IgG Alexa Fluor 594 (Thermo FisherScientific) in 1:200 dilution for 1 hour. After, washing 3 times with SP, 4′,6-diamidino-2-phenylindole (Dapi) was added and Vectashield mounting media (Vector) was added before placing the coverslip. Confocal images and Z-stacks were obtained using the Axio Observer.Z1 microscope with alpha Plan-Apochromat 63x/Oil DIC (UV) M27 (Zeiss). Digital images were captured using Axiocam MR R3 (Zeiss). Optical sections were then "stacked" or merged to create high resolution "z-series" images. Z-stack images were also portrayed as orthogonally projected on XY, YZ and XZ plane with maximum intensity using ZEN imaging software (Zeiss). A line was drawn through a representative cell to indicate relative intensity of RGB signals.

Mitochondrial length and area measurement

Live cell imaging was used to measure mitochondrial length and area of **c**ells grown on 35mm high glass-bottom μ-Dish tissue culture plates (MatTek Corp). The cells were washed with PBS and stained with 1μl of MitoView red (Biotium) in 5ml serum free DMEM for 30 minutes. The cells were then washed with PBS and refed with serum free DMEM and immediately live cell imaged using the Axio Observer.Z1 (Zeiss) microscope with alpha plan-apochromat 40x/Oil DIC (UV) M27 (Zeiss) in an environment chamber (5% CO_2; 37°C). Digital images were captured using Axiocam MR R3 (Zeiss). Mitochondrial length was measured by tracing the mitochondria from one end to the other with a line that was calibrated to the scale bar using

Image J software. Area was measured using Image J software according to Ouellet et al (Ouellet et al., 2017). Briefly, threshold was used to select the area of each mitochondria. The background was eliminated and using 'analyze particle', the area of each mitochondria was measured by considering the scale bar as the reference point. At least 100 mitochondria were measured for length and area from each of 3 different controls (Ctl) and p107KO c2MP cell lines. The measurements were categorized and graphed within different intervals of lengths and areas, respectively.

Cardiotoxin-induced muscle regeneration

Three-month-old anesthetized wild type and p107KO mice were injected intramuscularly in the tibialis anterior (TA) muscle with 40µl of cardiotoxin (ctx) Latoxan (Sigma) that was prepared by dissolving in water to a final concentration of 10µM. A day after ctx injury, bromodeoxyuridine (Brdu) at 100mg/kg was injected intraperitonially. TA muscles were collected on day 2 post ctx injection, immersed in a 1:2 ratio of 30% sucrose:optimal cutting temperature compound (ThermoFisher Scientific) solution and frozen slowly in liquid nitrogen-cooled isopentane. Mice were also untreated or treated with 750mg/kg ox for four consecutive days, with ctx on the third day and brdu on the fourth day, before the TA muscles were dissected on the fifth day for freezing.

Immunohistochemistry

The frozen samples were cross sectioned at 10µm thickness on a cryostat and mounted on positive charged slides (FroggaBio). Muscle tissue sections were washed with PBS and fixed with 4% paraformaldehyde (PFA) for 15 minutes at room temperature. 2N HCl was added for 20 minutes followed by 40mM sodium citrate for 10 minutes at room temperature. After washing in PBS, muscle sections were blocked in blocking buffer (5% goat serum, 0.1% Triton X in PBS) for 30 minutes. Muscle tissue sections were then incubated with primary antibody anti-MyoD (Novus Biologicals) in blocking buffer in 1:100 ratio overnight or p107-SD9 or

Pax7-EE8 in blocking buffer for 90 minutes. After three washes in 0.05% Tween 20 in PBS (PBST), cells were incubated with secondary antibody goat anti rabbit IgG Alexa Fluor 594 (ThermoFisher Scientific) or donkey anti-mouse IgG NL493-conjugated (R and D Systems) for one hour in 1:200 ratio. After three washes in PBST the tissue section was re-incubated with primary antibody Brdu-MoBU-1 (Santa Cruz Biotechnology) or Cox4 (Abcam) in blocking buffer in 1:100 ratio for 1 hour. After washing 3 times in PBST, the tissue section was incubated with secondary antibody donkey anti-mouse IgG NL493-conjugated (R and D Systems) or goat anti rabbit IgG Alexa Fluor 594 (ThermoFisher Scientific) in 1:200 ratio for 1 hour. After washing 3 times in PBST, Dapi was added and Vectashield mounting media (Vector) was added before placement of coverslip. The sample was imaged using confocal microscopy with the Axio Observer.Z1 microscope with alpha Plan-Apochromat 40x/Oil DIC (UV) M27 (Zeiss). Pax7 positive proliferating MPs containing p107 co-localized with Cox4 were identified in successive tissue sections that were cut at 6μm instead of 10μm. Proliferating MPs were determined by enumerating the $MyoD^{+}Brdu^{+}Dapi^{+}$ cells as a percentage of all the $Dapi^{+}$ cells per field. Six fields per muscle section from 4 to 5 different mice for each treatment was used for the analysis.

Growth curve and Proliferation Rate

3000 cells were plated for both control and p107KO c2MPs that were untreated or treated with 2.5mM ox. On each of the following 3 days, the number of cells were counted and graphed. Proliferation rate was calculated from the slope of the cell proliferation over time.

Flow Cytometry

For cell cycle analysis 50000, Ctl and p107KO cells were treated or untreated with 2.5mM ox for 40hrs or Ctl and Sirt1 KO cells were grown in 5.5mM glucose, to activate Sirt1, for 20 hours or p107KO cells 24 hours post transfection with pCMV6-OCT-HA-eGFP alone or together with p107fl or p107mls were used. The cells were washed twice with PBS by

centrifuging at 1200g for 5 minutes and re-dissolved in 1ml of PBS. Cells were then fixed by adding the cell suspension dropwise to 9ml of 70% ethanol while vortexing and then kept at -20°C overnight. The next day, the fixed cells were pelleted at 4000 rpm for 5 minutes and resuspended with 3ml PBS on ice for 10 minutes to rehydrate the cells. The rehydrated cells were centrifuged at 4000 rpm for 5 minutes and dissolved in 500µl of PBS containing 50µg/ml propidium iodide (ThermoFisher Scientific) and 25µg/ml RNAse (ThermoFisher Scientific) before loading on the Attune Nxt Flow Cytometer (ThermoFisher Scientific). Forward and side scatter were appropriately adjusted and propidium iodide was excited with the 488-nm laser and detected in the BL2 channel. The excitation was analyzed by the ModFit LT™ software that provided the percentage of cells present in each of G1, S and G2 phases of cell cycle, which were represented graphically. Flow cytometry for cell cycle analysis of transfected cells consisted of cells transfected with empty vector pCMV6-OCT-HA-eGFP expressing GFP alone or along with p107fl expressing full length p107 or with p107mls expressing full length p107, which is directed to the mitochondria. GFP positive cells were first sorted using the BL1 channel of the cytometer by adjusting forward and side scatter, followed by detection of propidium iodide that was excited with the 488-nm laser and detected in the BL2 channel The excitation was analyzed by the ModFit LT™ software that provided the percentage of cells present in each of G1, S and G2 phases of cell cycle and represented graphically.

Live cell ATP analysis (Seahorse)

3000 control or p107KO cells or p107KO cells 24 hours post transfection with pCMV6-OCT-HA-eGFP alone or together with p107fl or p107mls were seeded in DMEM (Wisent) containing 10% FBS and 1% penicillin streptomycin on microplates (Agilent Technologies) and treated according to the required experiment. For analysis, cells were washed in XF assay media supplemented with 10mM glucose, 1mM pyruvate and 2mM glutamine (Agilent Technologies) and incubated in a CO_2 free incubator in the same media at 37°C for 1 hour. The

media was then removed and replenished with fresh XF media supplemented with 10mM glucose, 1mM pyruvate and 2mM glutamine and the microplate was assessed using the Seahorse XF real-time ATP rate assay kit (Agilent Technologies) on a Seahorse XFe96 extracellular flux analyzer (Agilent Technologies), with addition of 1.5µM of oligomycin and 0.5µM rotenone + antimycin A as per the manufacturer's direction. The energy flux data in real time was determined using Wave 2.6 software.

Statistical analysis

Statistical analysis was performed by GraphPad Prism. Student's t-tests were used unless otherwise stated. Results were considered to be statistically significant when $p < 0.05$. Specific data was analyzed using an appropriate one-way or two-way analysis of variance (ANOVA) with a criterion of $p < 0.05$. All significant differences for ANOVA testing were evaluated using a Tukey post hoc test. All data are mean ± SD.

References

Bhattacharya, D., and Scime, A. (2020). Mitochondrial Function in Muscle Stem Cell Fates. Front Cell Dev Biol *8*, 480.

Bhattacharya, D., Ydfors, M., Hughes, M.C., Norrbom, J., Perry, C.G., and Scime, A. (2017). Decreased transcriptional corepressor p107 is associated with exercise-induced mitochondrial biogenesis in human skeletal muscle. Physiol Rep *5*.

Boily, G., He, X.H., Pearce, B., Jardine, K., and McBurney, M.W. (2009). SirT1-null mice develop tumors at normal rates but are poorly protected by resveratrol. Oncogene *28*, 2882-2893.

Bustin, S.A., Benes, V., Garson, J.A., Hellemans, J., Huggett, J., Kubista, M., Mueller, R., Nolan, T., Pfaffl, M.W., Shipley, G.L.*, et al.* (2009). The MIQE guidelines: minimum information for publication of quantitative real-time PCR experiments. Clin Chem *55*, 611-622.

Canto, C., Menzies, K.J., and Auwerx, J. (2015). NAD(+) Metabolism and the Control of Energy Homeostasis: A Balancing Act between Mitochondria and the Nucleus. Cell Metab *22*, 31-53.

Cerletti, M., Jang, Y.C., Finley, L.W., Haigis, M.C., and Wagers, A.J. (2012). Short-term calorie restriction enhances skeletal muscle stem cell function. Cell Stem Cell *10*, 515-519.

Cerutti, R., Pirinen, E., Lamperti, C., Marchet, S., Sauve, A.A., Li, W., Leoni, V., Schon, E.A., Dantzer, F., Auwerx, J.*, et al.* (2014). NAD(+)-dependent activation of Sirt1 corrects the phenotype in a mouse model of mitochondrial disease. Cell Metab *19*, 1042-1049.

Chen, D., Livne-bar, I., Vanderluit, J.L., Slack, R.S., Agochiya, M., and Bremner, R. (2004). Cell-specific effects of RB or RB/p107 loss on retinal development implicate an intrinsically death-resistant cell-of-origin in retinoblastoma. Cancer Cell *5*, 539-551.

Dali-Youcef, N., Mataki, C., Coste, A., Messaddeq, N., Giroud, S., Blanc, S., Koehl, C., Champy, M.F., Chambon, P., Fajas, L.*, et al.* (2007). Adipose tissue-specific inactivation of the retinoblastoma protein protects against diabesity because of increased energy expenditure. Proc Natl Acad Sci U S A *104*, 10703-10708.

De Sousa, M., Porras, D.P., Perry, C.G., Seale, P., and Scime, A. (2014). p107 is a crucial regulator for determining the adipocyte lineage fate choices of stem cells. Stem Cells *32*, 1323-1336.

Fajas, L. (2013). Re-thinking cell cycle regulators: the cross-talk with metabolism. Front Oncol *3*, 4.

Folmes, C.D., Nelson, T.J., Dzeja, P.P., and Terzic, A. (2012). Energy metabolism plasticity enables stemness programs. Ann N Y Acad Sci *1254*, 82-89.

Foster, D.A., Yellen, P., Xu, L., and Saqcena, M. (2010). Regulation of G1 Cell Cycle Progression: Distinguishing the Restriction Point from a Nutrient-Sensing Cell Growth Checkpoint(s). Genes Cancer *1*, 1124-1131.

Fulco, M., Cen, Y., Zhao, P., Hoffman, E.P., McBurney, M.W., Sauve, A.A., and Sartorelli, V. (2008). Glucose restriction inhibits skeletal myoblast differentiation by activating SIRT1 through AMPK-mediated regulation of Nampt. Dev Cell *14*, 661-673.

Fulco, M., Schiltz, R.L., Iezzi, S., King, M.T., Zhao, P., Kashiwaya, Y., Hoffman, E., Veech, R.L., and Sartorelli, V. (2003). Sir2 regulates skeletal muscle differentiation as a potential sensor of the redox state. Molecular cell *12*, 51-62.

Gemin, A., Sweet, S., Preston, T.J., and Singh, G. (2005). Regulation of the cell cycle in response to inhibition of mitochondrial generated energy. Biochem Biophys Res Commun *332*, 1122-1132.

Ghosh-Choudhary, S., Liu, J., and Finkel, T. (2020). Metabolic Regulation of Cell Fate and Function. Trends Cell Biol *30*, 201-212.

Gustafsson, C.M., Falkenberg, M., and Larsson, N.G. (2016). Maintenance and Expression of Mammalian Mitochondrial DNA. Annu Rev Biochem *85*, 133-160.

Iwahori, S., Umana, A.C., VanDeusen, H.R., and Kalejta, R.F. (2017). Human cytomegalovirus-encoded viral cyclin-dependent kinase (v-CDK) UL97 phosphorylates and inactivates the retinoblastoma protein-related p107 and p130 proteins. J Biol Chem *292*, 6583-6599.

Jones, R.A., Robinson, T.J., Liu, J.C., Shrestha, M., Voisin, V., Ju, Y., Chung, P.E., Pellecchia, G., Fell, V.L., Bae, S.*, et al.* (2016). RB1 deficiency in triple-negative breast cancer induces mitochondrial protein translation. J Clin Invest *126*, 3739-3757.

Khacho, M., Clark, A., Svoboda, D.S., Azzi, J., MacLaurin, J.G., Meghaizel, C., Sesaki, H., Lagace, D.C., Germain, M., Harper, M.E., *et al.* (2016). Mitochondrial Dynamics Impacts Stem Cell Identity and Fate Decisions by Regulating a Nuclear Transcriptional Program. Cell Stem Cell *19*, 232-247.
Lapuente-Brun, E., Moreno-Loshuertos, R., Acin-Perez, R., Latorre-Pellicer, A., Colas, C., Balsa, E., Perales-Clemente, E., Quiros, P.M., Calvo, E., Rodriguez-Hernandez, M.A., *et al.* (2013). Supercomplex assembly determines electron flux in the mitochondrial electron transport chain. Science *340*, 1567-1570.
LeCouter, J.E., Kablar, B., Hardy, W.R., Ying, C., Megeney, L.A., May, L.L., and Rudnicki, M.A. (1998). Strain-dependent myeloid hyperplasia, growth deficiency, and accelerated cell cycle in mice lacking the Rb-related p107 gene. Mol Cell Biol *18*, 7455-7465.
Leng, X., Noble, M., Adams, P.D., Qin, J., and Harper, J.W. (2002). Reversal of growth suppression by p107 via direct phosphorylation by cyclin D1/cyclin-dependent kinase 4. Mol Cell Biol *22*, 2242-2254.
Lindeman, G.J., Gaubatz, S., Livingston, D.M., and Ginsberg, D. (1997). The subcellular localization of E2F-4 is cell-cycle dependent. Proc Natl Acad Sci U S A *94*, 5095-5100.
Locasale, J.W., and Cantley, L.C. (2011). Metabolic flux and the regulation of mammalian cell growth. Cell Metab *14*, 443-451.
Lu, G., Sun, H., Korge, P., Koehler, C.M., Weiss, J.N., and Wang, Y. (2009). Functional characterization of a mitochondrial Ser/Thr protein phosphatase in cell death regulation. Methods in enzymology *457*, 255-273.
Martinez-Reyes, I., and Chandel, N.S. (2020). Mitochondrial TCA cycle metabolites control physiology and disease. Nature communications *11*, 102.
Martinez-Reyes, I., Diebold, L.P., Kong, H., Schieber, M., Huang, H., Hensley, C.T., Mehta, M.M., Wang, T., Santos, J.H., Woychik, R., *et al.* (2016). TCA Cycle and Mitochondrial Membrane Potential Are Necessary for Diverse Biological Functions. Molecular cell *61*, 199-209.
Mendelsohn, B.A., Bennett, N.K., Darch, M.A., Yu, K., Nguyen, M.K., Pucciarelli, D., Nelson, M., Horlbeck, M.A., Gilbert, L.A., Hyun, W., *et al.* (2018). A high-throughput screen of real-time ATP levels in individual cells reveals mechanisms of energy failure. PLoS Biol *16*, e2004624.
Mishra, P., Carelli, V., Manfredi, G., and Chan, D.C. (2014). Proteolytic cleavage of Opa1 stimulates mitochondrial inner membrane fusion and couples fusion to oxidative phosphorylation. Cell Metab *19*, 630-641.
Mishra, P., and Chan, D.C. (2016). Metabolic regulation of mitochondrial dynamics. J Cell Biol *212*, 379-387.
Mitra, K., Wunder, C., Roysam, B., Lin, G., and Lippincott-Schwartz, J. (2009). A hyperfused mitochondrial state achieved at G1-S regulates cyclin E buildup and entry into S phase. Proc Natl Acad Sci U S A *106*, 11960-11965.
Muller, H., Moroni, M.C., Vigo, E., Petersen, B.O., Bartek, J., and Helin, K. (1997). Induction of S-phase entry by E2F transcription factors depends on their nuclear localization. Mol Cell Biol *17*, 5508-5520.
Myers, M.J., Shepherd, D.L., Durr, A.J., Stanton, D.S., Mohamed, J.S., Hollander, J.M., and Alway, S.E. (2019). The role of SIRT1 in skeletal muscle function and repair of older mice. J Cachexia Sarcopenia Muscle *10*, 929-949.
Newman, L.E., Schiavon, C., and Kahn, R.A. (2016). Plasmids for variable expression of proteins targeted to the mitochondrial matrix or intermembrane space. Cell Logist *6*, e1247939.
Ochocki, J.D., and Simon, M.C. (2013). Nutrient-sensing pathways and metabolic regulation in stem cells. J Cell Biol *203*, 23-33.
Ouellet, M., Guillebaud, G., Gervais, V., Lupien St-Pierre, D., and Germain, M. (2017). A novel algorithm identifies stress-induced alterations in mitochondrial connectivity and inner membrane structure from confocal images. PLoS Comput Biol *13*, e1005612.
Petrov, P.D., Ribot, J., Lopez-Mejia, I.C., Fajas, L., Palou, A., and Bonet, M.L. (2016). Retinoblastoma Protein Knockdown Favors Oxidative Metabolism and Glucose and Fatty Acid Disposal in Muscle Cells. J Cell Physiol *231*, 708-718.

Porras, D.P., Abbaszadeh, M., Bhattacharya, D., D'Souza, N.C., Edjiu, N.R., Perry, C.G.R., and Scime, A. (2017). p107 Determines a Metabolic Checkpoint Required for Adipocyte Lineage Fates. Stem Cells *35*, 1378-1391.
Rathbone, C.R., Booth, F.W., and Lees, S.J. (2009). Sirt1 increases skeletal muscle precursor cell proliferation. Eur J Cell Biol *88*, 35-44.
Rodier, G., Makris, C., Coulombe, P., Scime, A., Nakayama, K., Nakayama, K.I., and Meloche, S. (2005). p107 inhibits G1 to S phase progression by down-regulating expression of the F-box protein Skp2. J Cell Biol *168*, 55-66.
Rodriguez-Enriquez, S., Vital-Gonzalez, P.A., Flores-Rodriguez, F.L., Marin-Hernandez, A., Ruiz-Azuara, L., and Moreno-Sanchez, R. (2006). Control of cellular proliferation by modulation of oxidative phosphorylation in human and rodent fast-growing tumor cells. Toxicol Appl Pharmacol *215*, 208-217.
Ryall, J.G., Dell'Orso, S., Derfoul, A., Juan, A., Zare, H., Feng, X., Clermont, D., Koulnis, M., Gutierrez-Cruz, G., Fulco, M.*, et al.* (2015). The NAD(+)-dependent SIRT1 deacetylase translates a metabolic switch into regulatory epigenetics in skeletal muscle stem cells. Cell Stem Cell *16*, 171-183.
Salazar-Roa, M., and Malumbres, M. (2017). Fueling the Cell Division Cycle. Trends Cell Biol *27*, 69-81.
Scime, A., Grenier, G., Huh, M.S., Gillespie, M.A., Bevilacqua, L., Harper, M.E., and Rudnicki, M.A. (2005). Rb and p107 regulate preadipocyte differentiation into white versus brown fat through repression of PGC-1alpha. Cell Metab *2*, 283-295.
Scime, A., Soleimani, V.D., Bentzinger, C.F., Gillespie, M.A., Le Grand, F., Grenier, G., Bevilacqua, L., Harper, M.E., and Rudnicki, M.A. (2010). Oxidative status of muscle is determined by p107 regulation of PGC-1a. J Cell Biol *190*, 651-662.
Sweet, S., and Singh, G. (1995). Accumulation of human promyelocytic leukemic (HL-60) cells at two energetic cell cycle checkpoints. Cancer Res *55*, 5164-5167.
Tang, A.H., and Rando, T.A. (2014). Induction of autophagy supports the bioenergetic demands of quiescent muscle stem cell activation. The EMBO journal *33*, 2782-2797.
van den Bogert, C., van Kernebeek, G., de Leij, L., and Kroon, A.M. (1986). Inhibition of mitochondrial protein synthesis leads to proliferation arrest in the G1-phase of the cell cycle. Cancer Lett *32*, 41-51.
Vander Heiden, M.G., and DeBerardinis, R.J. (2017). Understanding the Intersections between Metabolism and Cancer Biology. Cell *168*, 657-669.
Verona, R., Moberg, K., Estes, S., Starz, M., Vernon, J.P., and Lees, J.A. (1997). E2F activity is regulated by cell cycle-dependent changes in subcellular localization. Mol Cell Biol *17*, 7268-7282.
Wang, L., Zhang, T., Xi, Y., Yang, C., Sun, C., and Li, D. (2016). Sirtuin 1 promotes the proliferation of C2C12 myoblast cells via the myostatin signaling pathway. Mol Med Rep *14*, 1309-1315.
Wheaton, W.W., Weinberg, S.E., Hamanaka, R.B., Soberanes, S., Sullivan, L.B., Anso, E., Glasauer, A., Dufour, E., Mutlu, G.M., Budigner, G.S.*, et al.* (2014). Metformin inhibits mitochondrial complex I of cancer cells to reduce tumorigenesis. Elife *3*, e02242.
Wirt, S.E., and Sage, J. (2010). p107 in the public eye: an Rb understudy and more. Cell Div *5*, 9.
Zacksenhaus, E., Shrestha, M., Liu, J.C., Vorobieva, I., Chung, P.E.D., Ju, Y., Nir, U., and Jiang, Z. (2017). Mitochondrial OXPHOS Induced by RB1 Deficiency in Breast Cancer: Implications for Anabolic Metabolism, Stemness, and Metastasis. Trends Cancer *3*, 768-779.
Zhang, H., Ryu, D., Wu, Y., Gariani, K., Wang, X., Luan, P., D'Amico, D., Ropelle, E.R., Lutolf, M.P., Aebersold, R.*, et al.* (2016). NAD(+) repletion improves mitochondrial and stem cell function and enhances life span in mice. Science *352*, 1436-1443.
Zhu, L., van den Heuvel, S., Helin, K., Fattaey, A., Ewen, M., Livingston, D., Dyson, N., and Harlow, E. (1993). Inhibition of cell proliferation by p107, a relative of the retinoblastoma protein. Genes Dev *7*, 1111-1125.
Zini, N., Trimarchi, C., Claudio, P.P., Stiegler, P., Marinelli, F., Maltarello, M.C., La Sala, D., De Falco, G., Russo, G., Ammirati, G.*, et al.* (2001). pRb2/p130 and p107 control cell growth by multiple

strategies and in association with different compartments within the nucleus. J Cell Physiol *189*, 34-44.

Figure Legends

Fig 1. p107 is localized in the mitochondria of proliferating myogenic progenitors. (A) Representative Western blot of whole cell (W), cytoplasmic (C) and nuclear (N) fractions for p107, α-tubulin (cytoplasm loading control) and His3a (nucleus loading control) during proliferation. **(B)** Representative Western blot and graphical representation of cytoplasmic (Cyto) and mitochondrial (Mito) c2MP fractions for p107, α-tubulin and Cox4 (mitochondria loading control) during proliferation (G) and growth arrest (Ga), n=3, asterisks denote significance, $**p<0.01$, Student T-test. **(C)** Representative Western blot for p107, α-tubulin and Cox4, of c2MP whole cell and mitochondrial fractions including outer membrane (OM), inner membrane (IM), soluble inner membrane (IMS) and matrix (M) that were isolated in 250mM or 25mM sucrose buffer, treated and untreated with trypsin. Confocal immunofluorescence microscopy for p107, Cox4, Dapi and Merge of proliferating **(D)** Control (Ctl) and genetically deleted p107 (p107KO) c2MPs and **(G)** wild type (Wt) and p107KO primary (pr) MPs (scale bar 10μm). **(E)** and **(H)** A line was drawn through a representative cell to indicate relative intensity of RGB signals with the arrowheads pointing to areas of concurrent intensities **(F)** and **(I)** an orthogonal projection was generated by a Z-stack (100 nm interval) image set using the ZEN program (Zeiss) in the XY, XZ, and YZ planes. **(J)** Schematic for inducing in vivo satellite cell (SC) activation and MP proliferation in the tibialis anterior (TA) muscle with cardiotoxin (ctx) injury (MN is myonuclei). **(K)** Confocal immunofluorescence microscopic merged image of wild type (Wt) TA muscle section 2 days post injury for Pax7 (green) and Dapi (blue) and p107 (green), Cox4 (red) and Dapi (blue) and for p107KO TA muscle section for p107 (green), Cox4 (red) and Dapi (blue) (scale bar 20μm). Arrows denote Pax7 $^{+}$p107^{+}Cox4^{+} cells (scale bar 20μm).

Fig 2. p107 down regulates mitochondrial ATP generation capacity. (A) Graphical representation of relative p107 and IgG mitochondrial DNA promoter occupancy by qChIP analysis during proliferation (G) and growth arrest (Ga) in control (Ctl) and p107KO c2MPs, n=3; asterisks denote significance, $**p<0.01$; two-way Anova with post hoc Tukey. Not detected (N.D.). Gene expression analysis by qPCR of mitochondrial encoded genes *Nd2, Nd6, Cox*2 and *Atp6* for **(B)** c2MPs during G and Ga, n=3 and **(C)** Ctl and p107KO c2MPs n=4, and Wt and p107KO prMPs during proliferation, n=4; asterisks denote significance, $*p<0.05$; $**p<0.01$; Student T-test. **(D)** Representative Western blot of G compared to Ga, and Ctl compared to p107KO c2MPs for each electron transport chain complex (c) subunits, cI (NDUFB8), cII (SDHB), cIII (UQCRC2), cIV (MTCO) and cV (ATP5A). **(E)** ATP generation rate and capacity over time for isolated mitochondria from G and Ga c2MPs n=4 and for **(F)** Ctl and p107KO c2MPs, n=4. For rate, asterisks denote significance, $**p<0.01$, Student T-test. For capacity significance statistics see **Suppl. Table 1A and 1B**. Live cell metabolic analysis by Seahorse for oxygen consumption rate (OCR) with addition of oligomycin (olig) and antimycin A (ant), rotenone (rot) for **(G)** G and Ga c2MPs n=6-8 and **(H)** Ctl and p107KO c2MPs, n=4. **(I)** Representative confocal microscopy live cell image of stained mitochondria (MitoView Red) for Ctl and p107KO c2MPs. Graphical representation of mitochondria number per grouped **(J)** lengths and areas using image J quantification; n=3; significance denoted by ψ=p<0.05, π=p<0.01, κ=p<0.001, ϕ=p<0.0001; Student T-test.

Fig 3. p107 discerns the NAD^{+}/NADH ratio to regulate Oxphos. (A) Representative Western blot and graphical representation of cytoplasmic (Cyto) and mitochondrial (Mito) fractions for p107, α-tubulin (cytoplasm loading control) and Cox4 (mitochondria loading control) of c2MPs grown in stripped media (SM) containing only 1.0mM, 5.5mM or 25mM glucose (Glu), n=3, asterisks denote significance, $*p<0.05$; Student T-test. **(B)** Graphical

representation of relative p107 and IgG mitochondrial DNA promoter occupancy by qChIP analysis for control (Ctl) and p107KO c2MPs grown in SM containing only 5.5mM (LoGlu) or 25mM (HiGlu) glucose, n=3, asterisks denote significance, ***p*<0.01; two-way Anova with post hoc Tukey. **(C)** Gene expression analysis by qPCR of mitochondrial encoded genes *Nd2, Nd6, Cox2* and *Atp6* for Ctl and p107KO c2MPs grown in SM containing LoGlu or HiGlu, n=4, asterisks denote significance, **p*<0.05, ***p*<0.01, *** *p*<0.001; two-way Anova with post hoc Tukey. **(D)** Gene expression analysis by qPCR of *Pgc-1α, Mfn2, Ant1* and *Nrf2* for c2MPs grown in SM containing LoGlu or HiGlu, n=3 (N.D. is not detected). **(E)** Mitochondrial DNA (mtDNA) to nuclear DNA (nDNA) ratio for c2MPs grown in SM containing LoGlu or HiGlu in the absence or presence of 5-aminoimidazole-4-carboxamide ribonucleotide (AICAR), n= 3. asterisks denote significance, **p*<0.05, ****p*<0.001; two-way Anova with post hoc Tukey. Isolated mitochondria ATP generation rate and capacity over time for **(F)** c2MPs (n =4) and **(G)** p107KO c2MPs (n =4), grown in SM containing LoGlu or HiGlu. For rate, asterisks denote significance, ***p*<0.01; Student T-test. For capacity significance statistics see Suppl. Table 1C. NAD^+/NADH ratio for **(H)** c2MPs grown in SM containing LoGlu or HiGlu. n=3 and **(I)** for c2MPs untreated (Unt) or treated with 2.5mM oxamate (ox), grown in 25mM glucose (Glu) or 10mM galactose (Gal) or with varying glutamine concentrations of 4mM (Gl4) or 20mM (Gl20), n=4, asterisks denote significance, ***p*<0.01, ****p*<0.001, *****p*<0.0001; Student T-test. **(J)** Representative Western blots and graphical representation of cytoplasmic (Cyto) and mitochondrial (Mito) fractions for p107, α-tubulin and Cox4 of cells in (I), n=3, asterisks denote significance, **p*<0.05**;** Student T-test. **(K)** qPCR analysis of cells in (I) for mitochondrial encoded gene expression of *Nd2, Nd6, Cox2* and *Atp6*. n=3, asterisks denote significance, **p*<0.05, ***p*<0.01, ****p*<0.001; Student T-test.

Fig 4. p107 is regulated by Sirt1. (A) Immunoprecipitation/Western blots for p107 and Sirt1 in control (Ctl) and p107KO c2MPs. (**B)** Representative Western blot of cytoplasmic (Cyto) and mitochondrial (Mito) fractions of p107, α-tubulin (α-tub) and Cox4 for Ctl and Sirt1KO c2MPs grown in stripped media with 5.5mM and 25mM glucose. **(C)** Gene expression analysis by qPCR of mitochondrial encoded genes *Nd2, Nd6, Cox2* and *Atp6* for Ctl and Sirt1KO c2MPs grown in stripped media with 5.5mM (LoGlu) and 25mM (HiGlu) glucose, n=4; asterisks denote significance, **p*<0.05, ***p*<0.01 **(D)** Isolated mitochondrial ATP generation rate and capacity over time for Ctl and Sirt1KO c2MPs grown in 5.5mM glucose. For rate n=4, asterisk denotes significance, **p*<0.05. For capacity significance statistics see Suppl. Table 1D **(E)** Representative Western blot of Cyto and Mito fractions for p107, α-tubulin and Cox4 of c2MPs untreated (Ctl) or treated with (10mM) Sirt1 inhibitor nicotinamide (nam) or **(K)** a concentration (10μM) of resveratrol (res) that activates Sirt1. Graphical representation of relative p107 and IgG mitochondrial DNA promoter occupancy by qChIP analysis in Ctl and p107KO c2MPs untreated (unt) or treated with **(F)** nam (n=3) and **(L)** a concentration of res (10μM) that activates Sirt1 (n=3), asterisks denote significance, **p*<0.05, ***p*<0.01; two-way Anova with post hoc Tukey. Gene expression analysis by qPCR of mitochondrial encoded genes *Nd2, Nd6, Cox2* and *Atp6* for Ctl, p107KO and Sirt1KO c2MPs unt and treated for **(G)** nam (n=4) and **(M)** a concentration (10μM) of res that activates Sirt1, (n=3-4); asterisks denote significance, **p*<0.05, ***p*<0.01, ****p*<0.001; Student T-test. Isolated mitochondria ATP generation rate and capacity over time for **(H)** Ctl and **(I)** Sirt1KO c2MPs treated and untreated with nam, n=4 or **(N)** Ctl and **(O)** Sirt1KO c2MPs treated or untreated with a concentration (10μM) of res that activates Sirt1, n=4. For rate asterisks denote significance, **p*<0.05, ***p*<0.01; Student T-test. For capacity significance statistics see Suppl. Table 1E and 1F. **(J)** Mitochondria DNA (mtDNA) to nuclear DNA (nDNA) ratio for c2MPs with and without AICAR and nam, n=3-4, asterisks denote significance, ****p*<0.001; Student T-test.

Fig 5. p107 directs the cell cycle rate through management of Oxphos generation. (A) Time course of treatments for wild type (Wt) and p107KO mice injected with cardiotoxin (ctx) and bromodeoxyuridine (Brdu). Endpoint representative confocal immunofluorescence microscopic merge image of MyoD (red), Brdu (green) and Dapi (blue) and graph depicting the percentage of proliferating myogenic progenitors from tibialis anterior muscle at day 2 post injury, n=4 asterisks denote significance, ***p<0.001; Student T-test. Arrows denote Brdu and MyoD positive nuclei. (scale bar 20μm) **(B)** Growth curve and proliferation rate during 3 days for control (Ctl) and p107KO c2MPs, n=6-8; asterisks denote significance, ***p<0.001, ****p<0.0001; Student T-test. **(C)** Cell cycle analysis by flow cytometry for Ctl, p107KO and Sirt1KO c2MPs, n=6-9; asterisks denote significance, *p<0.05; ***p<0.001 ****p<0.0001; Student T-test. **(D)** Representative Western blot of cytoplasmic (Cyto) and mitochondria (Mito) fractions for p107, α-tubulin and Cox4 of p107KO c2MPs that were transfected with empty vector alone or with full length p107 (p107fl) or mitochondria localized p107 (p107mls). **(E)** Cell cycle analysis by flow cytometry for cells in (D), n=6-9; asterisks denote significance, ***p<0.001, ****p<0.0001; Student T-test. **(F)** Live cell metabolic analysis of ATP production rate from mitochondria (Mito) and glycolysis (Glyc) and energetic map for Ctl and p107KO c2MPs, n=4-5; asterisks denote significance, *p<0.05, **p<0.01; two-way Anova and post hoc Tukey. **(G)** Gene expression analysis by qPCR of mitochondrial encoded genes *Nd2, Nd6, Cox2* and *Atp6* for Ctl and p107KO c2MPs in the presence or absence of oxamate (ox), n=4. asterisks denote significance, *p<0.01, **p<0.01, ***p<0.001, ****p<0.0001; two-way Anova and post hoc Tukey. **(H)** Representative Western blot for Ctl and p107KO c2MPs untreated or treated with ox for electron transport chain complex. **(I)** Live cell metabolic analysis for ATP production of c2MPs untreated or treated with ox, n=6-8. **(J)** Growth curve, n=6-8, **(K)** proliferation rate, n=6-8, **(L)** Cell cycle analysis, n=6-8 for Ctl and p107KO c2MPs untreated or treated with ox; asterisks and symbols denote significance, ***p<0.001, ****p<0.0001 and ψ<0.05, κ<0.001, ϕ<0.0001. **(M)** Time course treatments for Wt and p107KO mice injected with ox, ctx and Brdu with Endpoint representative confocal immunofluorescence merge of MyoD (red), Brdu (green) and Dapi (blue) (scale bar 20μm). Arrows denote Brdu and MyoD positive nuclei and **(N**) graph depicting the percentage of proliferating MPs from tibialis anterior muscle at day 2 post injury, n=5; asterisks denote significance, *p<0.05, ****p<0.001; two-way Anova with post hoc Tukey.

Figure 1

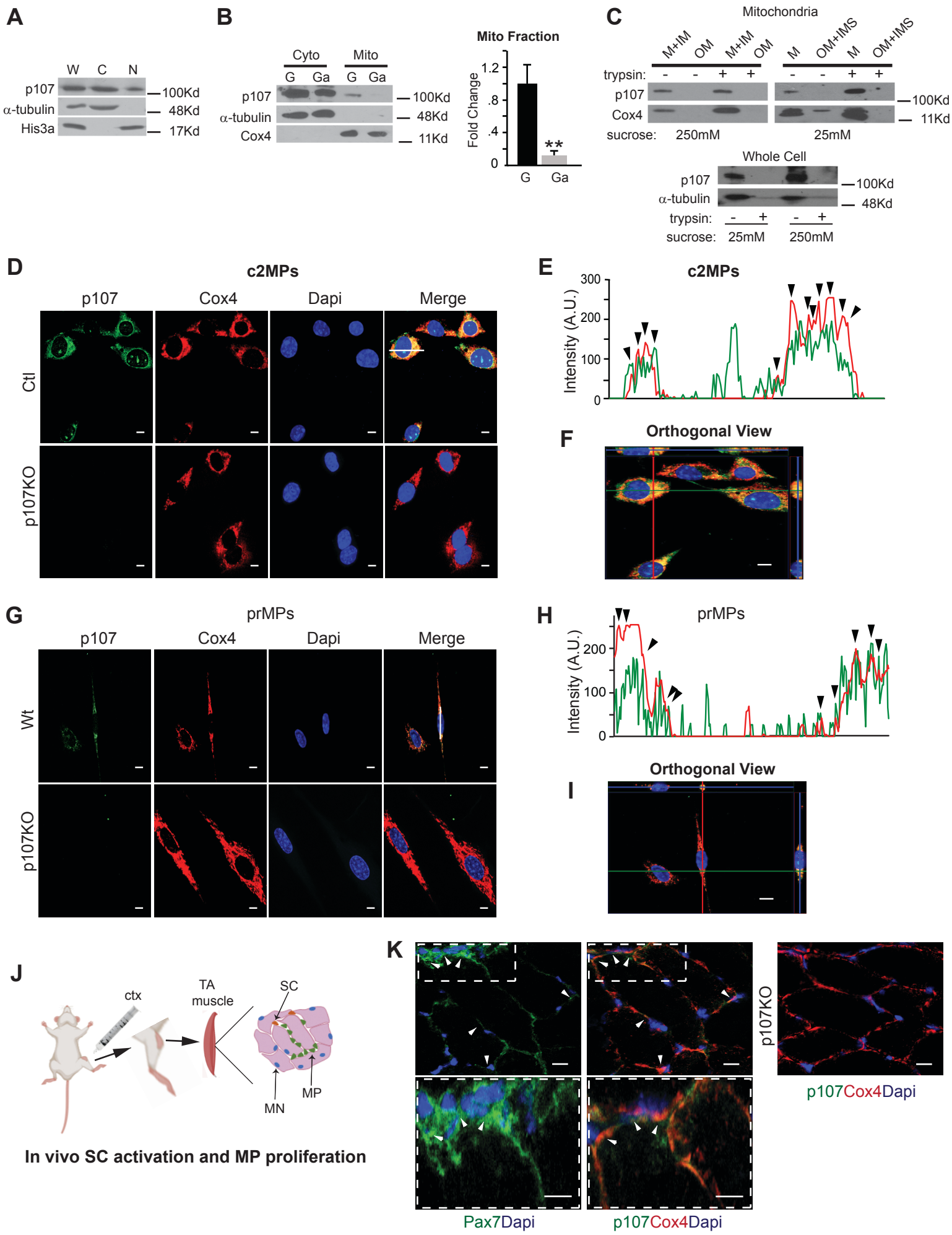
A
W C N
p107
α-tubulin
His3a
100Kd
48Kd
17Kd
B
Cyto
Mito
G Ga G Ga
p107
α-tubulin
Cox4
100Kd
48Kd
11Kd
Mito Fraction
Fold Change
1.2
.8
.4
0
**
G Ga
C
Mitochondria
M+IM OM M+IM OM M OM+IMS M OM+IMS
trypsin: - - + + - - + +
p107
Cox4
100Kd
11Kd
sucrose: 250mM 25mM
Whole Cell
p107
α-tubulin
100Kd
48Kd
trypsin: - + - +
sucrose: 25mM 250mM
D
c2MPs
p107 Cox4 Dapi Merge
Ctl
p107KO
E
c2MPs
Intensity (A.U.)
300
200
100
0
F
Orthogonal View
G
prMPs
p107 Cox4 Dapi Merge
Wt
p107KO
H
prMPs
Intensity (A.U.)
200
100
0
I
Orthogonal View
J
ctx
TA muscle
SC
MN
MP
In vivo SC activation and MP proliferation
K
p107KO
p107Cox4Dapi
Pax7Dapi
p107Cox4Dapi

Figure 2

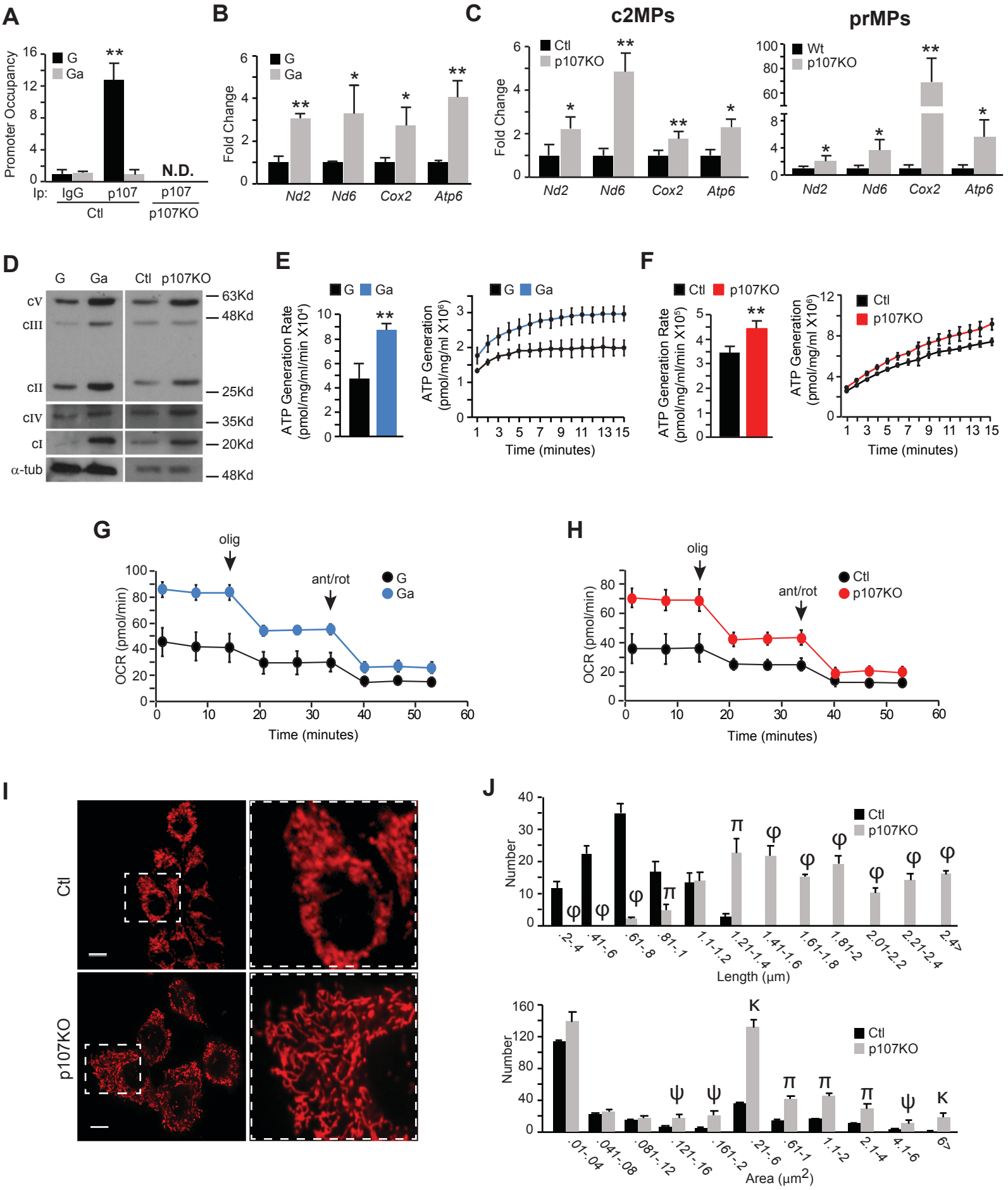
A
Promoter Occupancy
G
Ga
N.D.
Ip: IgG p107 p107
Ctl p107KO
B
Fold Change
Nd2 Nd6 Cox2 Atp6
C
c2MPs
prMPs
Ctl
p107KO
Wt
D
G Ga Ctl p107KO
cV
cIII
cII
cIV
cI
α-tub
63Kd
48Kd
25Kd
35Kd
20Kd
48Kd
E
ATP Generation Rate (pmol/mg/ml/min X10⁴)
ATP Generation (pmol/mg/ml X10⁶)
Time (minutes)
F
ATP Generation Rate (pmol/mg/ml/min X10⁵)
G
olig
ant/rot
OCR (pmol/min)
H
I
Ctl
p107KO
J
Number
Length (μm)
Area (μm²)

Figure 3

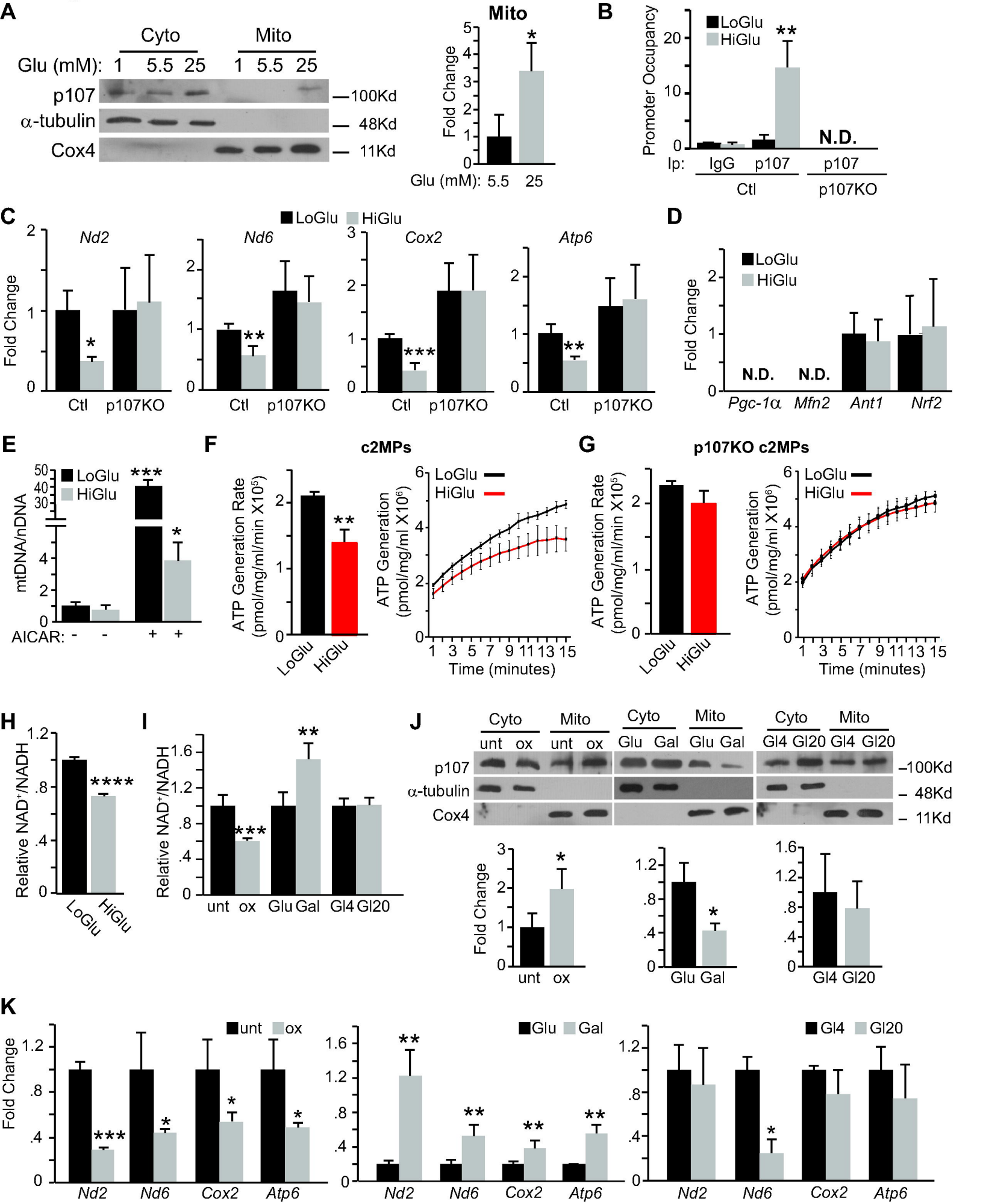
A
Cyto
Mito
Glu (mM): 1 5.5 25 1 5.5 25
p107
α-tubulin
Cox4
100Kd
48Kd
11Kd
Mito
Fold Change
Glu (mM): 5.5 25
B
LoGlu
HiGlu
Promoter Occupancy
N.D.
Ip: IgG p107 p107
Ctl
p107KO
C
LoGlu
HiGlu
Nd2
Nd6
Cox2
Atp6
Fold Change
Ctl p107KO
D
LoGlu
HiGlu
Fold Change
N.D. N.D.
Pgc-1α Mfn2 Ant1 Nrf2
E
LoGlu
HiGlu
mtDNA/nDNA
AICAR: - - + +
F
c2MPs
ATP Generation Rate (pmol/mg/ml/min X10^5)
LoGlu HiGlu
ATP Generation (pmol/mg/ml X10^6)
Time (minutes)
G
p107KO c2MPs
ATP Generation Rate (pmol/mg/ml/min X10^5)
LoGlu HiGlu
ATP Generation (pmol/mg/ml X10^6)
Time (minutes)
H
Relative NAD+/NADH
LoGlu HiGlu
I
Relative NAD+/NADH
unt ox Glu Gal Gl4 Gl20
J
Cyto Mito Cyto Mito Cyto Mito
unt ox unt ox Glu Gal Glu Gal Gl4 Gl20 Gl4 Gl20
p107
α-tubulin
Cox4
100Kd
48Kd
11Kd
Fold Change
unt ox
Glu Gal
Gl4 Gl20
K
unt ox
Glu Gal
Gl4 Gl20
Fold Change
Nd2 Nd6 Cox2 Atp6

Figure 4

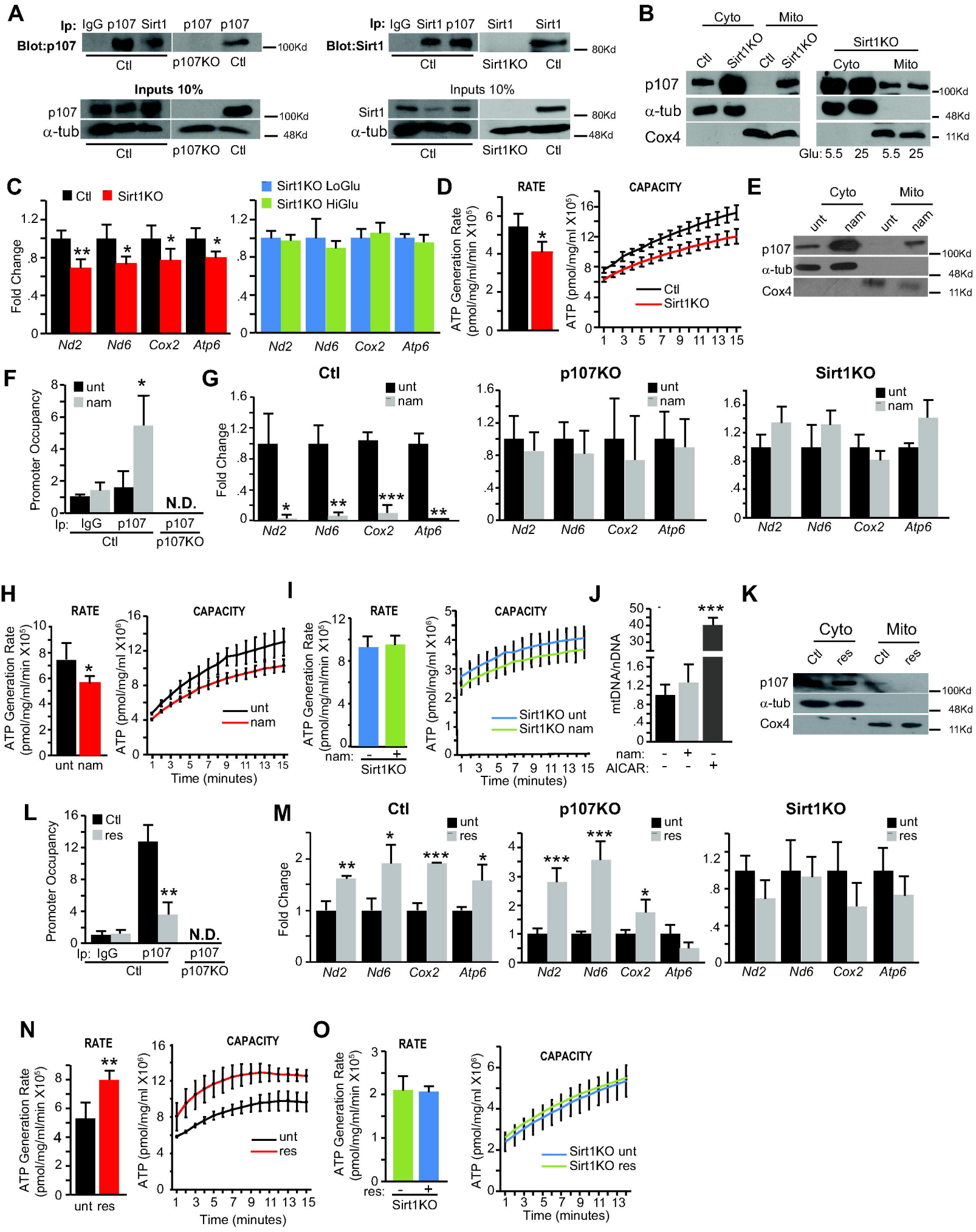
A
Ip: IgG p107 Sirt1 p107 p107
Blot:p107
Ctl p107KO Ctl
Inputs 10%
p107
α-tub
100Kd
48Kd
Ip: IgG Sirt1 p107 Sirt1 Sirt1
Blot:Sirt1
Ctl Sirt1KO Ctl
80Kd
B
Cyto Mito
Ctl Sirt1KO Ctl Sirt1KO
Sirt1KO
Cyto Mito
p107
α-tub
Cox4
100Kd
48Kd
11Kd
Glu: 5.5 25 5.5 25
C
Ctl Sirt1KO
Fold Change
Nd2 Nd6 Cox2 Atp6
Sirt1KO LoGlu
Sirt1KO HiGlu
D
RATE
CAPACITY
ATP Generation Rate (pmol/mg/ml/min X10^5)
ATP (pmol/mg/ml X10^6)
Ctl
Sirt1KO
E
Cyto Mito
unt nam unt nam
p107
α-tub
Cox4
100Kd
48Kd
11Kd
F
unt
nam
Promoter Occupancy
N.D.
Ip: IgG p107 p107
Ctl p107KO
G
Ctl
p107KO
Sirt1KO
unt
nam
Fold Change
Nd2 Nd6 Cox2 Atp6
H
RATE
CAPACITY
ATP Generation Rate (pmol/mg/ml/min X10^5)
ATP (pmol/mg/ml X10^6)
unt nam
Time (minutes)
I
RATE
CAPACITY
ATP Generation Rate (pmol/mg/ml/min X10^5)
ATP (pmol/mg/ml X10^6)
nam: - +
Sirt1KO
Sirt1KO unt
Sirt1KO nam
Time (minutes)
J
mtDNA/nDNA
nam: - + -
AICAR: - - +
K
Cyto Mito
Ctl res Ctl res
p107
α-tub
Cox4
100Kd
48Kd
11Kd
L
Ctl
res
Promoter Occupancy
N.D.
Ip: IgG p107 p107
Ctl p107KO
M
Ctl
p107KO
Sirt1KO
unt
res
Fold Change
Nd2 Nd6 Cox2 Atp6
N
RATE
CAPACITY
ATP Generation Rate (pmol/mg/ml/min X10^5)
ATP (pmol/mg/ml X10^6)
unt res
Time (minutes)
O
RATE
CAPACITY
ATP Generation Rate (pmol/mg/ml/min X10^5)
ATP (pmol/mg/ml X10^6)
res: - +
Sirt1KO
Sirt1KO unt
Sirt1KO res
Time (minutes)

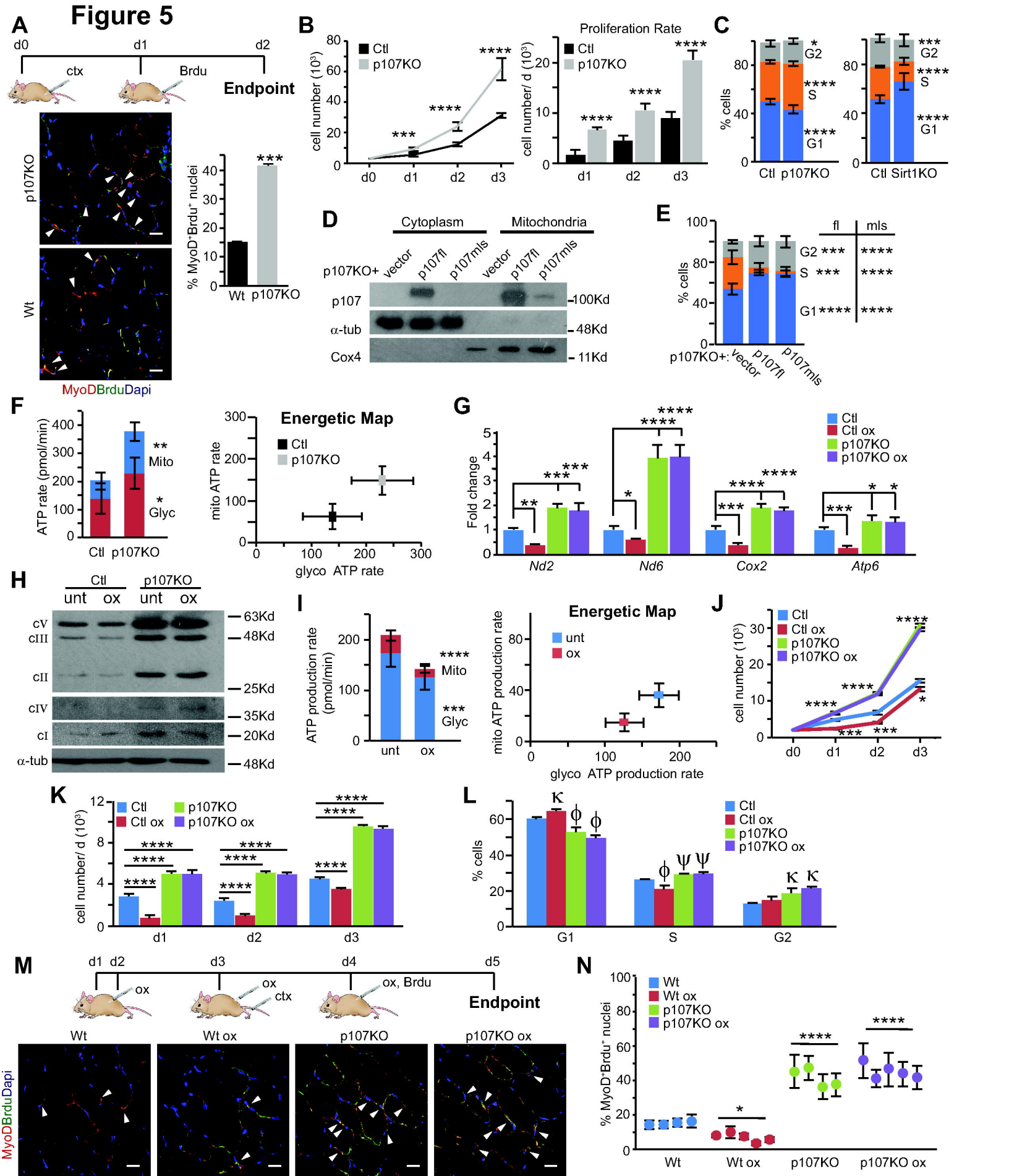
Figure 5
A
d0
d1
d2
ctx
Brdu
Endpoint
p107KO
Wt
MyoDBrduDapi
% MyoD+Brdu+ nuclei
Wt
p107KO
B
Ctl
p107KO
cell number (10³)
Proliferation Rate
cell number/ d (10³)
d0
d1
d2
d3
C
% cells
G2
S
G1
Ctl
p107KO
Sirt1KO
D
Cytoplasm
Mitochondria
p107KO+
vector
p107fl
p107mls
p107
α-tub
Cox4
100Kd
48Kd
11Kd
E
fl
mls
% cells
G2
S
G1
p107KO+:
vector
p107fl
p107mls
F
ATP rate (pmol/min)
Mito
Glyc
Ctl
p107KO
Energetic Map
mito ATP rate
glyco ATP rate
G
Fold change
Ctl
Ctl ox
p107KO
p107KO ox
Nd2
Nd6
Cox2
Atp6
H
Ctl
p107KO
unt
ox
cV
cIII
cII
cIV
cI
α-tub
63Kd
48Kd
25Kd
35Kd
20Kd
48Kd
I
ATP production rate (pmol/min)
Mito
Glyc
unt
ox
Energetic Map
mito ATP production rate
glyco ATP production rate
J
cell number (10³)
d0
d1
d2
d3
K
cell number/ d (10³)
d1
d2
d3
L
% cells
G1
S
G2
M
d1
d2
d3
d4
d5
ox
ox
ctx
ox, Brdu
Endpoint
Wt
Wt ox
p107KO
p107KO ox
MyoDBrduDapi
N
% MyoD+Brdu+ nuclei
Wt
Wt ox
p107KO
p107KO ox